

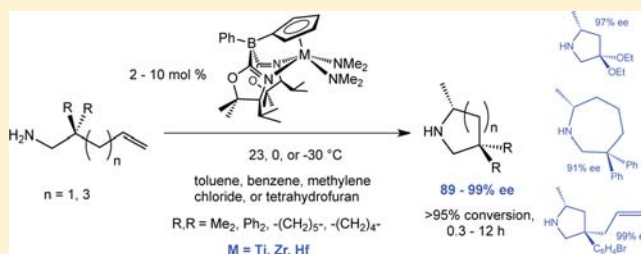
Highly Enantioselective Zirconium-Catalyzed Cyclization of Aminoalkenes

Kuntal Manna, William C. Everett, George Schoendorff, Arkady Ellern, Theresa L. Windus, and Aaron D. Sadow*

Department of Chemistry and U.S. Department of Energy Ames Laboratory, Iowa State University, Ames, Iowa 50011, United States

S Supporting Information

ABSTRACT: Aminoalkenes are catalytically cyclized in the presence of cyclopentadienylobis(oxazoliny)borato group 4 complexes $\{\text{PhB}(\text{C}_5\text{H}_4)(\text{Ox}^R)_2\}\text{M}(\text{NMe}_2)_2$ ($\text{M} = \text{Ti}, \text{Zr}, \text{Hf}$; $\text{Ox}^R = 4,4$ -dimethyl-2-oxazoline, 4*S*-isopropyl-5,5-dimethyl-2-oxazoline, 4*S*-*tert*-butyl-2-oxazoline) at room temperature and below, affording five-, six-, and seven-membered N-heterocyclic amines with enantiomeric excesses of >90% in many cases and up to 99%. Mechanistic investigations of this highly selective system employed synthetic tests, kinetics, and stereochemistry. Secondary aminopentene cyclizations require a primary amine (1–2 equiv vs catalyst). Aminoalkenes are unchanged in the presence of a zirconium monoamido complex $\{\text{PhB}(\text{C}_5\text{H}_4)(\text{Ox}^{4*S*-i\text{Pr},\text{Me}_2})_2\}\text{Zr}(\text{NMe}_2)\text{Cl}$ or a cyclopentadienylmono(oxazoliny)borato zirconium diamide $\{\text{Ph}_2\text{B}(\text{C}_5\text{H}_4)(\text{Ox}^{4*S*-i\text{Pr},\text{Me}_2})\}\text{Zr}(\text{NMe}_2)_2$. Plots of initial rate versus [substrate] show a rate dependence that evolves from first-order at low concentration to zero-order at high concentration, and this is consistent with a reversible substrate–catalyst interaction preceding an irreversible step. Primary kinetic isotope effects from substrate conversion measurements ($k'_{\text{obs}}(\text{H})/k'_{\text{obs}}(\text{D}) = 3.3 \pm 0.3$) and from initial rate analysis ($k_2(\text{H})/k_2(\text{D}) = 2.3 \pm 0.4$) indicate that a N–H bond is broken in the turnover-limiting and irreversible step of the catalytic cycle. Asymmetric hydroamination/cyclization of *N*-deutero-aminoalkenes provides products with higher optical purities than obtained with *N*-proteo-aminoalkenes. Transition state theory, applied to the rate constant k_2 that characterizes the irreversible step, provides activation parameters consistent with a highly organized transition state ($\Delta S^\ddagger = -43(7) \text{ cal}\cdot\text{mol}^{-1} \text{ K}^{-1}$) and a remarkably low enthalpic barrier ($\Delta H^\ddagger = 6.7(2) \text{ kcal}\cdot\text{mol}^{-1}$). A six-centered, concerted transition state for C–N and C–H bond formation and N–H bond cleavage involving two amidoalkene ligands is proposed as most consistent with the current data.



INTRODUCTION

The pursuit of optically active amines is motivated by their importance in commodity and specialty chemicals, medicinal compounds, and natural products.¹ Although enantioselective olefin hydroamination is potentially a powerful and efficient approach for amine synthesis, significant challenges remain.² Regio- and stereochemical control for additions of aliphatic alkenes and amines is currently limited; few catalysts provide terminal amine products (anti-Markovnikov addition) without control from directing groups, and intermolecular Markovnikov addition reactions are typically poorly enantioselective. Products with high optical purities are limited to a few choice pyrrolidines even in the well-studied intramolecular hydroamination/cyclization; asymmetric olefin hydroaminations that afford functionalized pyrrolidines, piperidines, and azapanes (among many valuable chiral N-heterocycles) are not yet developed.

Still, great progress is highlighted by advances with metallocene-based and axially chiral lanthanide catalysts,^{3–11} alkali metal coordination complexes,¹² and alkaline earth metal catalysts.¹³ Breakthroughs in zirconium-catalyzed alkene hydroamination include axially chiral bis(aryloxy),¹⁴ bis(amido),¹⁵ a

highly enantioselective bis(amidate)^{16–18} and bis-(carboxamide)¹⁹ complexes (or similar Ta-based systems)²⁰ as catalysts. C_1 -symmetric mixed $\text{Cp}^*(\text{oxazoliny} \text{ aryloxy})$ -zirconium and constrained geometry-type catalysts uniquely depart from the predominant axially chiral ligand design.²¹ Few highly enantioselective late-transition-metal-catalyzed aminopentene cyclizations have been reported.²² Although the enantioselective systems have been generally limited to pyrrolidines, highly efficient and selective intramolecular catalysts may provide strategies for addressing some of the tougher challenges in olefin hydroamination.

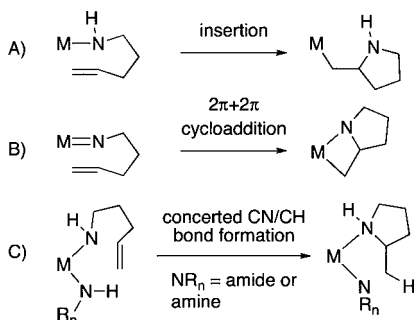
In this context, catalyst synthesis, substrate screening, and mechanistic tests may further advance the field. Detailed studies that probe hydroamination/cyclization mechanisms have focused on d^0 or $f^0 d^0$ complexes including rare earth,^{6d,11,23,24} actinide,²⁵ alkaline earth metal,^{26–28} titanium,²⁹ and zirconium.^{25,30–32} Typically, the catalytic cycles associated with these species are proposed to have metal-amido resting states. From that point, the proposed mechanisms for C–N bond

Received: January 7, 2013

Published: April 30, 2013

formation are remarkably divergent to include (A) olefin insertion into a $[M]-NR_2$ bond and (B) $[2\pi + 2\pi]$ cycloaddition of olefin and $[M]=NR$ involving four-centered metallacyclic intermediates. Recently, (C) a concerted C–N and C–H bond-forming mechanism was proposed to involve a six-centered transition state (Scheme 1).

Scheme 1. Proposed Pathways for C–N Bond Formation in d^0 and $f^0 d^0$ Metal-Catalyzed Aminopentene Cyclization

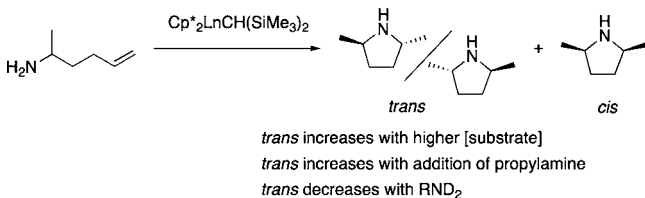


Additionally, modifications to the olefin insertion mechanism have included a proposal that the C–N bond formation is facilitated by a coordinated amine (proton-assisted insertion)³ and a suggestion that the bond-forming step is reversible based on a computational analysis.³³

Unfortunately, the experimental characteristics of most catalytic systems are similar, complicating mechanistic elucidation. For example, rate laws often show zero-order dependence on substrate concentration, irrespective of the proposed mechanism. Generally, reactions of N-deuterated amines are slower (i.e., there are primary isotope effects), and Eyring plots invariably indicate that transition states are highly ordered. Because these few characteristics describe most hydroamination/cyclization reactions, insight into subtle effects on rate and selectivity is often limited.

A few interesting observations, however, provide some guidance. First, diastereoselectivity in organolanthanide-catalyzed cyclization of racemic aminoalkenes is enhanced with high substrate concentration and through the addition of propylamine, but it is lowered with N-deuterated substrates (Scheme 2).²³

Scheme 2. Conditions That Influence the *cis/trans* Ratio in Cyclization of Racemic Aminoalkenes



Second, zero-order substrate dependence suggests a unimolecular turnover-limiting step, arguing strongly for the insertion mechanism (Scheme 1A), while the primary-in-magnitude isotope effect suggests that N–H bond cleavage occurs between the catalyst resting state and the turnover-limiting transition state.²³ Insertion of alkenes into $M-N$ bonds would not be expected to have a significant isotope effect. This contrast suggests that C–N bond formations may be

mechanistically distinct from other addition reactions involving unsaturated C–C moieties and M–E bonds (e.g., M–H).

Mechanistic assignments are further complicated in zirconium-catalyzed cyclizations by conflicting observations involving primary and secondary aminoalkenes as substrates for transformation by cationic and neutral catalysts. Cationic catalyst systems, such as $Cp_2ZrMe_2/B(C_6F_5)_3$, are only active for secondary aminoalkenes, and catalyst deactivation with primary amines is proposed to involve formation of inactive, neutral zirconium imidoalkene species.^{14,34} In contrast, several neutral zirconium complexes cyclize primary, but not secondary, aminoalkenes; this observation is often invoked as support for a zirconium imido intermediate prior to $[2\pi + 2\pi]$ cycloaddition. Notably, this reaction pathway for imidozirconium compounds and olefins (B in Scheme 1) is not independently established (although $[Zr]=NR$ and alkyne cycloadditions are well-known).³⁵ In fact, mixtures of an isolated zirconium imido and alkenes return starting materials.³⁶ Furthermore, an interesting dipyrrolylmethane zirconium compound cyclizes both primary and secondary aminoalkenes.³⁷

Likewise, isolation of the organometallic metal–alkylamine product from olefin insertion has not yet been described for a d^0 or $f^0 d^0$ metal amido compound. However, the zirconium vinylamine product of alkyne insertion into a zirconium–nitrogen bond was recently isolated and characterized.³⁸ In addition, a molybdenum amido and alkyne react to provide a d^2 molybdenum vinylamine.³⁹ Interestingly, strong support for olefin insertion into d^n metal amidos ($n \neq 0$) has been provided in palladium systems,^{40,41} and an early catalytic hydroamination reaction involves norbornene insertion into an $[Ir]-NHP$ bond.⁴²

These unusual features, as well as the potential for amine synthesis, motivated our initial investigations of zirconium-catalyzed aminoalkene cyclization using an achiral cyclopentadienylbis(oxazolonyl)borate ligand.³² A second-order rate law ($-d[\text{aminopentene}]/dt = k[Zr]^1[\text{aminopentene}]^1$) and primary isotope effect were rationalized through reversible substrate addition, but compelling evidence ruling out “incorrect” pathways was not available. As noted above, many early transition-metal hydroaminations are plagued by similar mechanistic ambiguity.

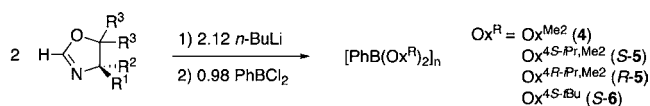
Stereochemistry provides an additional tool for assessing the mechanism; therefore, we prepared optically active compounds containing chiral oxazolines. The resulting zirconium compounds are remarkably active and highly enantioselective.⁴³ This system is characterized by a number of interesting observations, including the nonlinear correlation between substrate concentration and cyclization rate, the requirement that the substrate/catalyst ratio should be >2 for catalytic turnover, the positive effect of N-deuteriation on the enantiomeric excess of the product, and the observation that cyclization of secondary aminoalkenes requires a primary amine additive. These observations are inconsistent with $[2\pi + 2\pi]$ cycloaddition and insertion pathways (A and B, Scheme 1). Instead, we proposed concerted C–N and C–H bond formation through a two-substrate intermediate involving a six-centered transition state. A similar pathway was suggested but ultimately excluded for a related zirconium catalyst.³⁰ In addition, two-substrate pathways have been proposed for magnesium and calcium,^{26,27b,c,28} rare earth,^{11,24} and zirconium catalysts.³¹

Here we describe a detailed investigation of this group-4-based system for asymmetric hydroamination. We have studied the precatalyst structures, pursued structure/activity/selectivity relationships for precatalysts and substrate combinations, and correlated these observations with kinetic effects to better understand this highly active and highly enantioselective system for C–N bond formation.

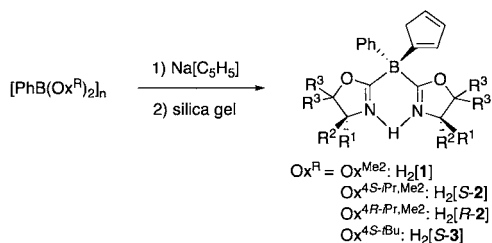
RESULTS

1. Synthesis and Characterization of Oxazolinylboranes and Oxazolinylborates. Four dianionic cyclopentadienylobis(oxazolinyl)borates are prepared as diprotonated species (Scheme 3).^{11,32,43} The compounds H[PhB(C₅H₅)-

Scheme 3. Synthesis of Achiral and Chiral Oxazolinylboranes and Cyclopentadienylobis(oxazolinyl)borates



Ox^{Me2}: R¹=R²=Me; R³=H
 Ox^{4*S*-iPr,Me2}: R¹=H; R²=*i*-Pr; R³=Me
 Ox^{4*R*-iPr,Me2}: R¹=*i*-Pr; R²=H; R³=Me
 Ox^{4*S*-tBu}: R¹=R³=H; R²=*t*-Bu



(Ox^R)₂] (H₂[1]; Ox^{Me2} = 4,4-dimethyl-2-oxazoline), H₂[S-2]; Ox^{4*S*-iPr,Me2} = 4*S*-isopropyl-5,5-dimethyl-2-oxazoline), H₂[R-2]; Ox^{4*R*-iPr,Me2} = 4*R*-isopropyl-5,5-dimethyl-2-oxazoline), H₂[S-3]; Ox^{4*S*-tBu} = 4*S*-*tert*-butyl-2-oxazoline) are synthesized in two steps from the appropriate 2*H*-oxazolines 2*H*-Ox^R via neutral bis(oxazolinyl)phenylborane PhB(Ox^R)₂ intermediates 4,⁴⁴ S-5, R-5, and S-6.

The ¹¹B and ¹⁵N NMR chemical shifts and infrared C=N stretching frequencies for 4, S-5, and S-6 are listed in Table 1. The ¹¹B NMR values are consistent with neutral, four-coordinate boron centers and suggest that a neutral donor (i.e., acetonitrile-*d*₃) coordinates to the boron center.⁴⁵

The bis(oxazolinyl)phenylboranes 4–6 react with Na[C₅H₅] in THF to provide the desired mixed cyclopentadienyloxazolinylborates H[PhB(C₅H₅)(Ox^R)₂] after chromatography. Isolated H₂[1], H₂[S-2], H₂[R-2], and H₂[S-3] are obtained as mixtures of three isomers, as indicated by ¹H and ¹¹B NMR spectroscopy (Table 1). The ¹H NMR spectra of these mixtures were complicated by overlapping resonances in the phenyl, cyclopentadienyl, and oxazoline regions and were not useful for characterization or assessment of purity. ¹¹B NMR spectroscopy was more informative, and the three resonances in the ¹¹B NMR spectrum of achiral 1 were upfield compared to that of borane 4 (as an acetonitrile adduct), as expected.⁴⁵ The 1-C₅H₅(BR₃), 2-C₅H₅(BR₃), and 5-C₅H₅(BR₃) connectivity accounts for the three isomers. Borylcyclopentadienyl compounds are known to form mixtures of isomers.⁴⁶

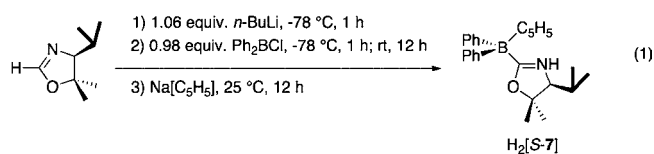
A chiral cyclopentadienylnono(oxazolinyl)diphenylborate, synthesized for comparison with the cyclopentadienylobis-

Table 1. ¹¹B (128 MHz) and ¹⁵N NMR (71 MHz) Chemical Shifts and ν_{CN} Values for Oxazoline-Containing Compounds

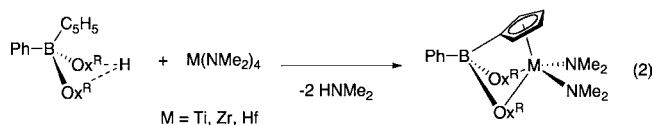
compound	¹¹ B NMR ^a	¹⁵ N NMR ^a	ν _{CN} ^b
H ₂ [PhBCp(Ox ^{Me2}) ₂] (H ₂ [1])	-15.3, -15.6, -16.0	-172.0	1589
H ₂ [PhBCp(Ox ^{4<i>S</i>-iPr,Me2}) ₂] (H ₂ [S-2])	-15.7	-179.1	1584, 1567
H ₂ [PhBCp(Ox ^{4<i>R</i>-iPr,Me2}) ₂] (H ₂ [R-2])	-15.7	-179.1	1582, 1560
H ₂ [PhBCp(Ox ^{4<i>S</i>-tBu}) ₂] (H ₂ [S-3])	-14.9, -15.3, -15.6	-190.9	1595, 1588
PhB(Ox ^{Me2}) ₂ (4)	-8.1	-147.0	1621, 1601
PhB(Ox ^{4<i>S</i>-iPr,Me2}) ₂ (S-5)	-7.5	-131.6	1588
PhB(Ox ^{4<i>S</i>-tBu}) ₂ (S-6)	-7.3	-124.3	1617, 1590
H ₂ [Ph ₂ BCp(Ox ^{4<i>S</i>-iPr,Me2}) ₂] (H ₂ [S-7])	-10.0, -11.5, -12.4	-155.2	1594
2 <i>H</i> -Ox ^{4<i>S</i>-iPr,Me2}	na	-143.3	1632
2 <i>H</i> -Ox ^{4<i>S</i>-tBu}	na	-148.0	1635

^aValue given in parts per million, measured in acetonitrile-*d*₃ solvent. ^bKBr, cm⁻¹.

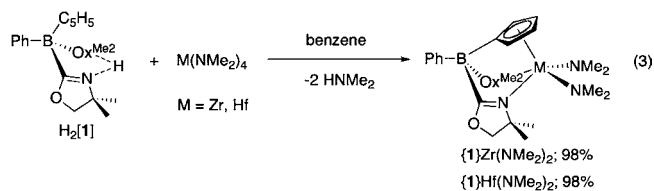
(oxazolinyl)borate ligands 1–3, is prepared by reaction of 2Li-Ox^{4*S*-iPr,Me2} and Ph₂BCl followed by addition of Na[C₅H₅]. Exhaustive purification by silica gel column chromatography yields H[Ph₂B(C₅H₅)(Ox^{4*S*-iPr,Me2})] (H₂[S-7]) in poor yield (eq 1). Three ¹¹B NMR resonances indicates that this cyclopentadienylnono(oxazolinyl)borate is also a mixture of three isomers.



2. Synthesis and Characterization of Cyclopentadienyloxazolinylborate Group 4 Compounds. The preparation of cyclopentadienyloxazolinylborate group 4 complexes involves reaction of homoleptic dimethylamide compounds M(NMe₂)₄ (M = Ti, Zr, Hf) and H₂[1], H₂[S-2], H₂[R-2], H₂[S-3], and H₂[7] (eq 2). However, the conditions for synthesis and the complex stability vary significantly for the metal–ligand pairs.



The achiral H₂[1] and M(NMe₂)₄ (M = Zr, Hf) react rapidly in benzene at room temperature, affording {PhB(C₅H₅)(Ox^{Me2})₂}M(NMe₂)₂ ({1}M(NMe₂)₂; eq 3). ¹H NMR spectra



of micromolar-scale experiments in benzene-*d*₆ indicated that the reactions proceeded to completion within 10 min.

Table 2. ^{15}N NMR (71 MHz) Chemical Shifts, ν_{CN} and $[\alpha]_{\text{D}}^{20}$ Values for Cyclopentadienylbis(oxazolinyl)borate Group 4 Complexes

compound	^{15}N NMR	ν_{CN}	$[\alpha]_{\text{D}}^{20}$
{PhBCP(Ox ^{Me₂}) ₂ }Zr(NMe ₂) ₂ ({1}Zr(NMe ₂) ₂); amorphous	-135	1595	na
{1}Zr(NMe ₂) ₂ ; crystallized	na	1603, 1505	na
{1}Zr(NMe ₂) ₂ THF; crystallized	na	1610, 1533	na
{1}Hf(NMe ₂) ₂	-132	1595	na
{PhBCP(Ox ^{4<i>S</i>-iPr,Me₂}) ₂ }Zr(NMe ₂) ₂ ({S-2}Zr(NMe ₂) ₂)	-153, -155	1565	-124.7°
{R-2}Zr(NMe ₂) ₂	-152, -155	1559	+122.6°
{S-2}Hf(NMe ₂) ₂	-149, -151	1559	-86.98°
{S-2}Ti(NMe ₂) ₂	-154, -156	1560	-94.71°
{PhBCP(Ox ^{4<i>S</i>-iBu}) ₂ }Zr(NMe ₂) ₂ ({S-3}Zr(NMe ₂) ₂)	-145, -148	1608, 1506	-139.1°
{S-2}Zr(NMe ₂)Cl	-153, -155	1578, 1567	-111.4°
{Ph ₂ BCP(Ox ^{4<i>S</i>-iPr,Me₂}) ₂ }Zr(NMe ₂) ₂ ({S-7}Zr(NMe ₂) ₂)	-155	1562	-82.0°

Analytically pure materials are obtained in 98% isolated yield for both zirconium and hafnium compounds by evaporation of benzene and the HNMe₂ byproduct.

The spectroscopic data for {1}Zr(NMe₂)₂ and {1}Hf(NMe₂)₂ are similar (Table 2). Upon coordination and amine elimination, the ^1H NMR multiplets associated with the three C₅H₅B isomers are replaced with two resonances assigned to C₅H₄B in a C_s-symmetric molecule. One set of oxazoline resonances was observed as two singlets for inequivalent methyl groups and two doublets for the inequivalent CH₂. This pattern is invariant in ^1H NMR spectra acquired at temperatures from 190 to 300 K in toluene-*d*₈. ^1H - ^{15}N HMBC experiments contained a correlation between oxazoline methyl and nitrogen, and the ^{15}N NMR chemical shifts for the oxazoline nitrogen in zirconium and hafnium compounds at -135 and -132 ppm are only slightly upfield of noncoordinated 2*H*-4,4-dimethyl-2-oxazoline (-127 ppm). For comparison, the ^{15}N NMR chemical shift of {κ³-PhB(Ox^{Me₂})₃}Zr(NMe₂)₃ is -140 ppm, in which tridentate oxazoline coordination to Zr is unambiguous.⁴⁷ In the current system, the small change in ^{15}N NMR data of complexes versus 2*H*-oxazoline does not distinguish two simultaneously coordinated oxazolines from one coordinated oxazoline rapidly exchanging with a pendent oxazoline. Analytically pure, amorphous {1}Zr(NMe₂)₂ and {1}Hf(NMe₂)₂, obtained by evaporation of frozen benzene solutions, were analyzed by IR spectroscopy. Only one ν_{CN} band was observed for either compound (both at 1595 cm⁻¹; KBr). From these data, either (a) the C₅H₄B group and both oxazolines are bonded to the metal center or (b) the C₅H₄B group and only one oxazoline are coordinated with the pendent oxazoline and coordinated oxazoline exchanging rapidly on the ^1H NMR time scale in solution and the IR time scale in the solid state.

A single-crystal X-ray diffraction study of {1}Zr(NMe₂)₂THF showed only one oxazoline coordinated to the zirconium center.³² The coordination geometry of zirconium is a squashed four-legged piano stool. The dimethylamide groups are transoid (N-Zr-N: 120.26°) as are the oxazoline and THF ligands (N-Zr-O: 159.4°). The site *trans* to the cyclopentadienyl ring is unoccupied.

The coordination modes of {1} in this structure and the structure of amorphous {1}Zr(NMe₂)₂ are not equivalent. In particular, ν_{CN} bands at 1610 cm⁻¹ (pendant oxazoline) and 1533 cm⁻¹ (Zr-Ox^{Me₂}) were observed for crystals from THF. Furthermore, the conformation of {1}Zr(NMe₂)₂THF in the solid state is not representative of the solution structure. At room temperature, the signals in the ^1H NMR spectrum of

{1}Zr(NMe₂)₂THF were identical to those of {1}Zr(NMe₂)₂ in the absence of THF and those of THF in the absence of {1}Zr(NMe₂)₂. Interestingly, the ^1H NMR spectrum of {1}Zr(NMe₂)₂THF at 190 K contained only two broad single resonances, one assigned to oxazoline methyl and the other to oxazoline methylene groups. The two methyl groups on each oxazoline are expected to remain chemically inequivalent at all temperatures, and a rigid structure for {1}Zr(NMe₂)₂(THF) should contain either two or four methyl signals (depending on the structure). Thus, the fluxional process is too fast on the ^1H NMR time scale to resolve a rigid structure. The hafnium analogue {1}Hf(NMe₂)₂ is also fluxional in the presence of 1 equiv of THF, and the room temperature resonances assigned to oxazoline methyl substituents and the methylene group coalesce into two broad singlets at 190 K.

We therefore pursued X-ray-quality crystals of THF-free {1}Zr(NMe₂)₂, which were obtained by slow diffusion of pentane into a toluene solution of {1}Zr(NMe₂)₂ cooled to 243 K (Figure 1). As in {1}Zr(NMe₂)₂THF, the oxazolinylborate ligand bonds to Zr through the C₅H₄B moiety and one oxazoline group (Zr1-N1, 2.255(1) Å), while the second

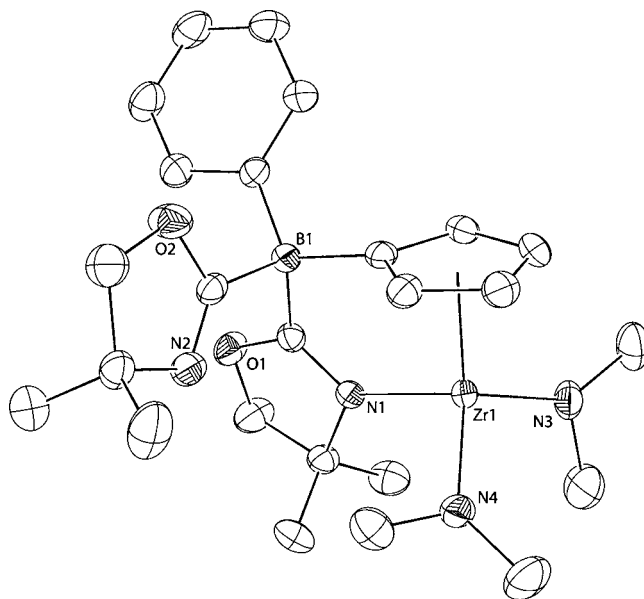
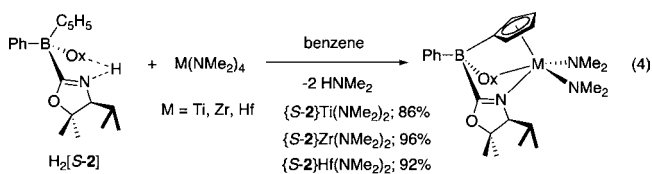


Figure 1. ORTEP diagram of {PhB(C₅H₄)(Ox^{Me₂})₂}Zr(NMe₂)₂ ({1}Zr(NMe₂)₂). Ellipsoids are plotted at 50% probability, and hydrogen atoms are not illustrated for clarity. Atomic distances (Å): Zr1-N1, 2.255(1); Zr1-N3, 2.031(2); Zr1-N4, 2.035(2).

oxazoline is not coordinated to Zr (Zr1–N2, 4.31 Å). The geometry at zirconium is that of a three-legged piano stool; the $\text{Cp}_{\text{centroid}}\text{--Zr--N1}$ angle (103.1°) is similar to that of the THF adduct, while the $\text{Cp}_{\text{centroid}}\text{--Zr--N3}$ and $\text{Cp}_{\text{centroid}}\text{--Zr--N4}$ angles (110.47 and 122.35°) are smaller than in $\{1\}\text{Zr}(\text{NMe}_2)_2\text{THF}$. The Zr–NMe₂ distances (Zr1–N3, Zr1–N4) are slightly shorter in $\{1\}\text{Zr}(\text{NMe}_2)_2$ than in the THF adduct (just outside of 3σ), and the Zr–N_{oxazoline} distance is 0.066 Å shorter in the THF-free species. We wished to identify whether this compound would provide the same IR spectrum as the material obtained from evaporation of benzene. In fact, the two spectra are inequivalent. A spectrum of the crystalline sample (KBr) contained two IR bands at 1603 and 1505 cm^{-1} assigned to ν_{CN} stretching frequencies of noncoordinated and Zr-coordinated oxazolines. These IR data contrast that of the material obtained by evaporation, where only one ν_{CN} band at 1595 cm^{-1} was observed.

In contrast to readily available Zr and Hf species, the reaction of $\text{Ti}(\text{NMe}_2)_4$ and $\text{H}_2[1]$ in benzene at room temperature provides a mixture of unidentified products. The ^1H NMR spectrum does not contain the same spectral signatures as noted above for $\{1\}\text{Zr}(\text{NMe}_2)_2$. Instead, ^1H NMR spectra of reaction mixtures in benzene-*d*₆ or toluene-*d*₈ contained vinylic resonances from isomers of $\text{C}_5\text{H}_5\text{B}$; the conversion of these signals to those associated with a single C_s -symmetric compound was not observed even upon heating at 120 °C. HNMe_2 was observed in spectra of reaction mixtures within 10 min, which indicated that some ligand substitution occurred. Four ^{11}B resonances were detected ranging from 33.6 to -14.7 ppm, and the upfield ^{11}B NMR signal suggested that a borane was among the reaction products.

Interestingly, the $\{S-2\}$ ligand supports a titanium complex as well as zirconium and hafnium compounds. The chiral, 4*S*-isopropyl-5,5-dimethyl-2-oxazoline-based $\text{H}_2[S-2]$ and $\text{M}(\text{NMe}_2)_4$ ($\text{M} = \text{Ti}, \text{Zr}, \text{Hf}$) react in benzene at room temperature, providing $\{S-2\}\text{M}(\text{NMe}_2)_2$ in excellent yield (eq 4; Ti: 25 h, 86%; Zr: 7 h, 96%; Hf: 7 h, 92%).



The opposite enantiomer $\{R-2\}\text{Zr}(\text{NMe}_2)_2$ is prepared from $\text{H}_2[R-2]$ and $\text{Zr}(\text{NMe}_2)_4$. As expected, the NMR and IR spectroscopic features of $\{S-2\}\text{Zr}(\text{NMe}_2)_2$ and $\{R-2\}\text{Zr}(\text{NMe}_2)_2$ are identical. Two sets of oxazoline resonances (e.g., two septets and four doublets assigned to the isopropyl groups and four singlets for the 5-methyl groups) and four downfield multiplets ranging from 6.7 to 6.06 ppm for the cyclopentadienyl group suggested C_1 -symmetric species for $\{S-2\}\text{Zr}(\text{NMe}_2)_2$ and $\{R-2\}\text{Zr}(\text{NMe}_2)_2$. Two singlets are observed for the two inequivalent dimethylamide ligands. Additionally, the broad ^{11}B NMR resonance at -15.7 ppm resulting from overlapping signals from isomers of $\text{H}_2[S-2]$ is replaced with a sharper signal at -14.5 ppm (122 Hz at half-height). The compounds $\{S-2\}\text{Ti}(\text{NMe}_2)_2$ and $\{S-2\}\text{Hf}(\text{NMe}_2)_2$ have similar ^1H NMR spectra. The C stereocenters in the molecule necessarily render the two oxazolines inequivalent, so ^1H NMR spectroscopy does not distinguish between zero-, one-, or two-coordinated oxazolines. However, ^{15}N NMR and IR spectroscopy

suggests that both oxazolines coordinate to the metal centers in $\{S-2\}\text{M}(\text{NMe}_2)_2$. Two ^{15}N NMR signals were observed at -152.6 and -155.0 in comparison to -143 for $2\text{H-Ox}^{4S-iPr,Me_2}$. Additionally, only one CN stretching frequency was observed in the IR at 1565 cm^{-1} (KBr). A ν_{CN} associated with a noncoordinated oxazoline, based on the higher energy ν_{CN} of $2\text{H-Ox}^{4S-iPr,Me_2}$ (1632 cm^{-1}), was not detected.

The solution structure of $\{S-2\}\text{Zr}(\text{NMe}_2)_2$ is further probed with a NOESY experiment to identify which groups on the ancillary ligand interact with the presumed reactive sites that are occupied by NMe₂ groups. The correlations and assignments are illustrated in Figure 2. First, the $\{S-2\}$ intraligand

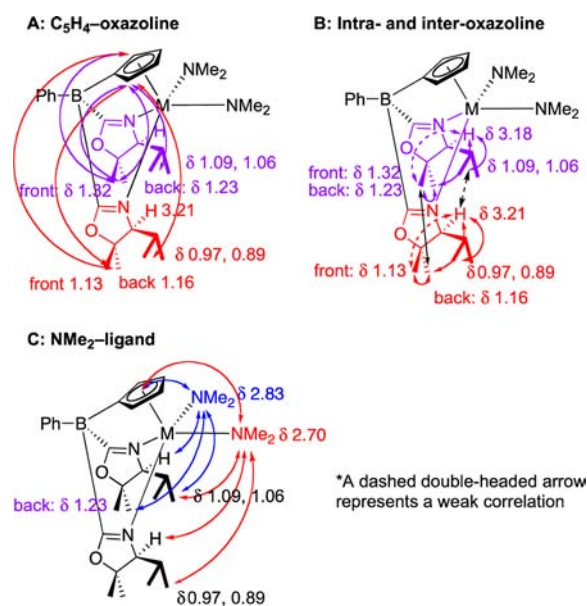
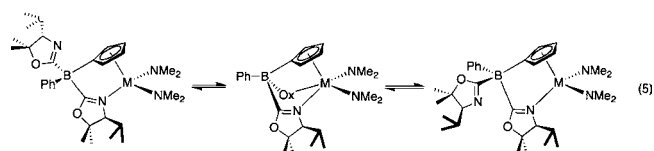


Figure 2. Correlations detected by NOESY experiments. The bidentate coordination mode is illustrated.

correlations establish the metal–ligand conformations that are populated sufficiently to provide NOEs (Figure 2A). The two sets of correlations discerned are oxazoline– C_5H_4 cross-peaks and oxazoline–oxazoline interactions.

Interestingly, the former correlations only involve the lateral 2- and 5-hydrogen on the C_5H_4 group (Figure 2A) to methyl and isopropyl groups of both oxazolines. No correlations between the oxazoline and the 3- and 4-hydrogen were observed in the NOESY. The lateral correlations suggest significant population of configurations in which the zirconium–ligand interaction contains one dissociated oxazoline $\{\eta^5\text{-}\kappa^1\text{-Ph}(\text{Ox}^{4S-iPr,Me_2})\text{B}(\text{C}_5\text{H}_4)(\text{Ox}^{4S-iPr,Me_2})\}\text{Zr}(\text{NMe}_2)_2$. This conformation is further supported by the X-ray crystal structure of $\{1\}\text{Zr}(\text{NMe}_2)_2$. However, there are also through-space correlations between the two oxazolines that suggest both oxazolines coordinate to zirconium in an isomer that exists on an NOE-significant time scale. Thus, we suggest that two conformations dominate the structure of $\{S-2\}\text{Zr}(\text{NMe}_2)_2$ and exchange rapidly on the NMR time scale (eq 5).



Furthermore, the intra- and interoxazoline correlations establish the relative orientation of the two oxazolines (Figure 2B). On the basis of the assignments and NOEs between oxazoline and NMe₂ ligands, we assign the signals for the inequivalent NMe₂ groups and the overall configuration of the zirconium center (Figure 2C). Interestingly, the “back” NMe₂ in Figure 2 at 2.83 ppm correlations show through-space interactions with only the back oxazoline, whereas the “front” NMe₂ at 2.70 ppm contained correlations with resonances from both oxazoline rings. Thus, the open space between the cyclopentadienyl and the back oxazoline is occupied by a dimethylamide group, and the other dimethylamide group is situated between the two oxazoline rings in the dicoordinated conformer.

To enhance the clarity of the presentation of through-space interactions, a rendered image is given in Figure 3. The zirconium–ligand interaction shows the C₁-symmetric environment that distinguishes the two NMe₂ groups.

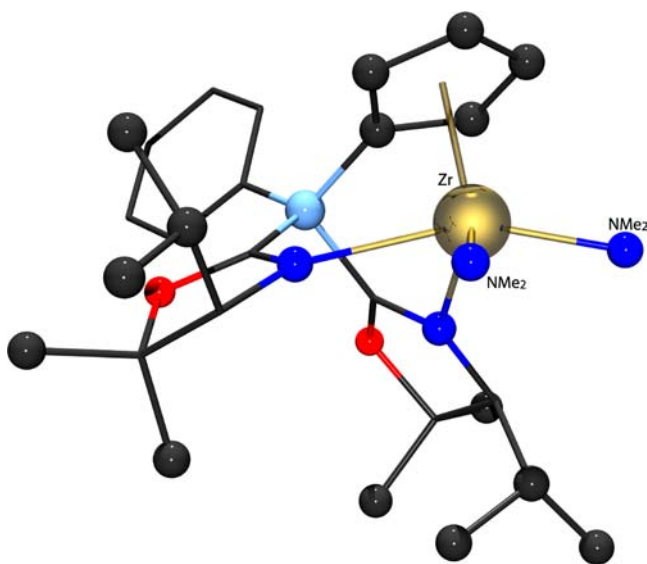
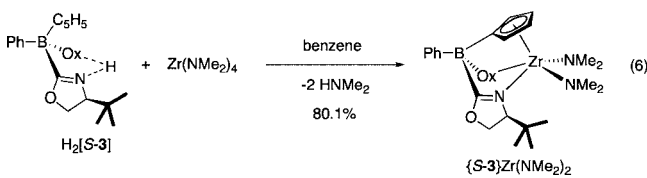


Figure 3. DFT-optimized $\{S-2\}Zr(NR_2)_2$ structure (B3LYP/3-21G). Hydrogen atoms and the amide substituents are not included for clarity. Nitrogens are depicted in blue, and the back NMe₂ group is significantly less hindered than the front group, according to NOESY experiments.

A second optically active zirconium complex $\{PhB(C_5H_4)(Ox^{4S-tBu})_2\}Zr(NMe_2)_2$ ($\{S-3\}Zr(NMe_2)_2$) is prepared by reaction of H₂[S-3] and Zr(NMe₂)₄ in benzene at room temperature for 20 min (eq 6).¹¹ In its ¹H NMR spectrum, two



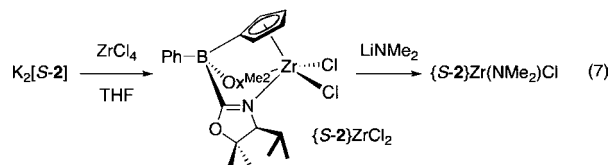
singlet resonances at 0.85 and 0.84 ppm were assigned to *tert*-butyl substituents on two inequivalent oxazoline groups, and four downfield multiplets ranging from 6.74 to 6.09 ppm were assigned to the cyclopentadienyl group. Likewise and as in S-2, two singlets for two inequivalent dimethylamido groups were observed, and the overall pattern was consistent with C₁ symmetry. In the ¹¹B spectrum, a sharp resonance at −14.4

ppm indicated that a single product formed. However, the complex $\{S-3\}Zr(NMe_2)_2$ decomposes in benzene at room temperature ($t_{1/2} = 2$ h), leading to HNMe₂ and unidentified oxazolinyborate products. In contrast, $\{S-2\}M(NMe_2)_2$ complexes (M = Ti, Zr, Hf) are unchanged in benzene even after 36 h at room temperature.

Additionally, several compounds were required to test the reactive valences required for hydroamination catalysis and the nature of ancillary ligand–zirconium interaction and its impact on cyclization and enantioselectivity. The compound $\{S-2\}Zr(NMe_2)Cl$ was prepared to address the former point. Reaction of H₂[S-2] and 2 equiv of KCH₂C₆H₅ affords K₂[S-2]. Reaction of K₂[S-2] and ZrCl₄ in THF at room temperature provides $\{S-2\}ZrCl_2$ within 30 min.

Four doublets and four singlets in the ¹H NMR spectrum (THF-*d*₈) assigned to oxazoline isopropyl and methyl groups were consistent with inequivalent oxazolines expected for a C₁-symmetric complex. Four multiplets in the downfield region from 6.88 to 6.23 ppm were attributed to the cyclopentadienyl group in $\{S-2\}ZrCl_2$. The complex is unchanged in THF-*d*₈ for 7 days at room temperature; however, broad signals were observed in ¹H NMR spectra of $\{S-2\}ZrCl_2$ after the solvent was evaporated and the residue was dissolved in THF-*d*₈. Therefore, the complex $\{S-2\}ZrCl_2$ is best prepared in situ for the synthesis of $\{S-2\}Zr(NMe_2)Cl$.

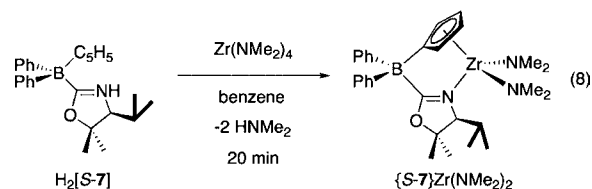
The desired compound $\{S-2\}Zr(NMe_2)Cl$ is prepared by addition of 1 equiv of LiNMe₂ to $\{S-2\}ZrCl_2$ (generated in situ, eq 7). The complex is isolated in 79% yield by evaporation of



the volatile materials from the reaction mixture, followed by benzene extraction. A mixture of two diastereomers is formed (in 4:1 ratio as detected by ¹H NMR spectroscopy of THF-*d*₈ solutions).

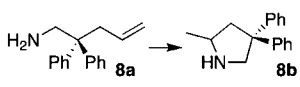
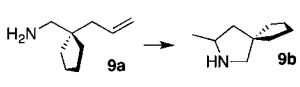
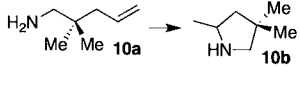
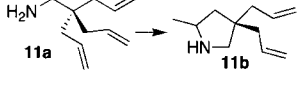
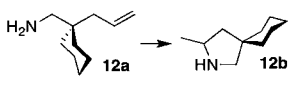
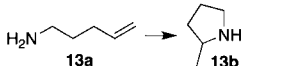
The ¹H NMR resonances associated with the ancillary ligand in each of the two diastereomers indicated the (expected) C₁-symmetry, although many of the resonances are overlapping. The 4:1 diastereomeric ratio remains unchanged in THF at room temperature after 12 h.

A mono(oxazoliny)borato zirconium $\{S-7\}Zr(NMe_2)_2$ compound is prepared by reaction of H[Ph₂B(C₅H₅)(Ox^{4S-iPr}Me₂)] and Zr(NMe₂)₄ in benzene at room temperature. $\{S-7\}Zr(NMe_2)_2$ is formed after 20 min and is isolated in 92% yield (eq 8).



The ¹H NMR spectrum of $\{S-7\}Zr(NMe_2)_2$ in benzene-*d*₆ is constant at room temperature over at least 12 h. One set of oxazoline resonances (i.e., one septet and two doublets assigned to the isopropyl groups and two singlets for the 5-methyl groups), two singlets for two inequivalent dimethylamido

Table 3. Catalytic Cyclization of Aminopentenes with Achiral and Optically Active Group 4 Compounds Coordinated by Mixed Cyclopentadienylbis(oxazolonyl)borato Ligands^a

Reactant to Product	Entry	Precatalyst	Solvent	Temp. (°C)	Time (h)	Yield (%) ^b	ee (%) ^c
	1	{1}Zr(NMe ₂) ₂	C ₆ H ₆	25	11	90 (84)	-
	2	{S-2}Zr(NMe ₂) ₂	C ₆ H ₆	25	1.25	95 (93)	93 (R)
	3	{S-2}Zr(NMe ₂) ₂	THF- <i>d</i> ₈	25	5	95	95 (R)
	4	{S-2}Zr(NMe ₂) ₂	CD ₂ Cl ₂	25	5	95	93 (R)
	5	{S-2}Zr(NMe ₂) ₂	C ₇ H ₈	-30	5 d	98	98 (R) ^d
	6	{R-2}Zr(NMe ₂) ₂	C ₆ H ₆	25	1.25	95	93 (S)
	7	{S-2}Hf(NMe ₂) ₂	C ₇ H ₈	0	15	98	97 (R) ^d
	8	{S-2}Ti(NMe ₂) ₂	C ₆ D ₆	25	5 d	93	76 (R)
	9	{S-3}Zr(NMe ₂) ₂	C ₆ H ₆	25	18	95 (89)	93 (R)
	10	{1}Zr(NMe ₂) ₂	C ₆ D ₆	25	11	88	-
	11	{S-2}Zr(NMe ₂) ₂	C ₆ H ₆	25	4	88 (81)	92 (R)
	12	{R-2}Zr(NMe ₂) ₂	C ₆ D ₆	25	4	88	92 (S)
	13	{S-2}Hf(NMe ₂) ₂	C ₇ D ₈	0	8	85	95 (R) ^d
	14	{S-3}Zr(NMe ₂) ₂	C ₆ D ₆	25	11	77	88 (R)
	15	{1}Zr(NMe ₂) ₂	C ₆ D ₆	25	11	85	-
	16	{S-2}Zr(NMe ₂) ₂	C ₆ H ₆	25	7	89 (82)	89 (R)
	17	{S-2}Zr(NMe ₂) ₂	C ₇ D ₈	-30	8 d	95	93 (R)
	18	{S-2}Hf(NMe ₂) ₂	C ₆ D ₆	25	20	90	87 (R)
	19	{1}Zr(NMe ₂) ₂	C ₆ D ₆	25	11	98	-
	20	{S-2}Zr(NMe ₂) ₂	C ₆ H ₆	25	0.75	98 (94)	92 (R)
	21	{S-2}Hf(NMe ₂) ₂	C ₇ H ₈	0	20	90 (85)	96 (R) ^d
	22	{S-2}Ti(NMe ₂) ₂	C ₆ D ₆	25	5 d	90	82 (R)
	23	{1}Zr(NMe ₂) ₂	C ₆ H ₆	25	11	92 (87)	-
	24	{S-2}Zr(NMe ₂) ₂	C ₆ H ₆	25	1.25	96 (88)	90 (R)
	25	{S-2}Zr(NMe ₂) ₂	THF- <i>d</i> ₈	0	11	92	94 (R)
	26	{R-2}Zr(NMe ₂) ₂	C ₆ D ₆	25	1.25	96	90 (S)
	27	{S-2}Hf(NMe ₂) ₂	C ₆ H ₆	25	5	95 (91)	93 (R)
	28	{S-2}Ti(NMe ₂) ₂	C ₆ D ₆	25	5 d	75	83 (R)
	29	{1}Zr(NMe ₂) ₂	C ₆ D ₆	25	15	90	-
	30	{S-2}Zr(NMe ₂) ₂	C ₆ D ₆	110	15	24	n.d.

^aReaction conditions: 10 mol % precatalyst. ^bIsolated yield is given in parentheses. ^cPercent enantiomeric excess ($\pm 0.5\%$) was determined by ¹H and/or ¹⁹F NMR spectroscopy of the Mosher amide derivatives. Absolute configuration assignments are based on literature reports.^{6d,16a} ^dPercent enantiomeric excess measured by ¹⁹F NMR of Mosher amide derivatives and also by HPLC of naphthoyl or benzylamide derivatives.

groups, and four downfield multiplets for the cyclopentadienyl group suggest a C₁-symmetric species for {S-7}Zr(NMe₂)₂. The ¹H NMR pattern was constant from 190 to 320 K in toluene-*d*₈. In the IR spectrum, one ν_{CN} at 1562 cm⁻¹ for {S-7}Zr(NMe₂)₂ indicates that the oxazoline is coordinated to the zirconium center.

3. Catalytic Hydroamination/Cyclization of Aminoalkenes. Cyclopentadienylbis(oxazolonyl)borato bis(amido) group 4 compounds catalyze the cyclization of aminoalkenes to give racemic and optically enriched pyrrolidine, piperidine, azepane, and indoline products at room temperature (Tables 3–5). These results are organized into tables by substrate type. Table 3 gives cyclization reactions of aminopentenes **8a**–**13a** that have aliphatic or aromatic 3,3-disubstitution; Table 4 contains six- and seven-membered rings from substrates **14a**–**16a**; Table 5 reports cyclizations of substrates **18a**–**22a** that give indolines as well as halogenated, acetal, and 2-ethyl-containing pyrrolidine products. In contrast, cyclization of aminoalkenes is not observed in the presence of monoamidic

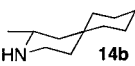
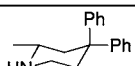
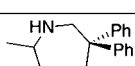
{S-2}Zr(NMe₂)Cl or mono-oxazoline {S-7}Zr(NMe₂)₂ under the conditions tested.

The rates of cyclization depend on the metal center, ancillary ligand, and substrate. Some general trends of catalytic rate (for which exceptions are identified below) are summarized as follows: first, the metal center affects the reaction rate following the trend Zr > Hf \gg Ti. Second, the ancillary ligand effect on cyclization rates of disubstituted aminoalkenes follows the trend {S-2}Zr(NMe₂)₂ > {1}Zr(NMe₂)₂ > {S-3}Zr(NMe₂)₂.

{S-2}Zr(NMe₂)₂ provides a more active catalyst than {S-2}Hf(NMe₂)₂. In many cases, only starting materials were detected in reactions of {S-2}Ti(NMe₂)₂ and aminopentenes (allowed to stand at room temperature for extended times). In fact, only three of the most highly reactive substrates, 2,2-diphenylpent-5-ene amine (**8a**), 2,2-bis(2-propenyl)-4-pentenylamine (**11a**), and C-(1-allylcyclohexyl)methylamine (**12a**), are cyclized by {S-2}Ti(NMe₂)₂ at room temperature with appreciable conversion.

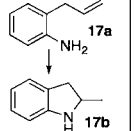
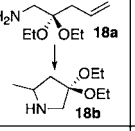
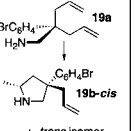
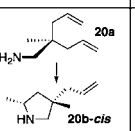
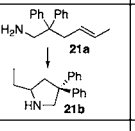
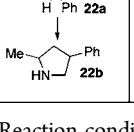
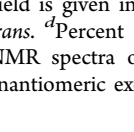
For zirconium catalysts, the oxazoline substituents affect hydroamination rates, generally following the trend {S-

Table 4. Catalytic Hydroamination/Cyclization of Aminohexenes and Aminoheptenes^a

Product	No.	Precat.	Time	% Yield ^b	% ee ^c
 14b	1	{1}Zr	11 h	87 (80)	-
	2	{S-2}Zr	40 h	48	31 ^e
	3	{S-2}Hf	30 h	85 ^d	26 ^e
	4	{S-3}Zr	48 h	80	29 ^e
 15b	5	{1}Zr	4 d	95 (89)	-
	6	{S-2}Zr	4 d	65	46
	7	{S-2}Hf	20 h	89 ^d	18
 16b	8	{1}Zr	5 d	56	-
	9	{S-2}Zr	5 d	73 (64)	91

^aReaction conditions: 10 mol % precatalyst, benzene, room temperature. ^bIsolated yield is given in parentheses. ^cPercent enantiomeric excess was determined by ¹⁹F NMR spectroscopy of the (*R*)-Mosher amide derivatives. ^dAt 85 °C. ^ePercent enantiomeric excess measured by HPLC.

Table 5. Catalytic Hydroamination/Cyclization of Functionalized Aminoalkenes^a

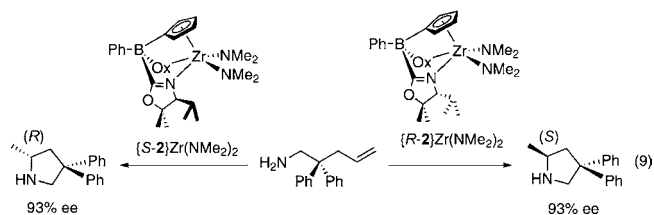
Reaction	No.	Precat.	Time	% Yield ^{b,c}	% ee ^d
 17a 17b	1	{1}Zr	3 d	90	-
	2	{S-2}Zr	3 d	92 (85)	95
	3	{S-2}Hf	5 d	80	94
 18a 18b	4	{1}Zr	30 h	90	-
	5	{S-2}Zr	30 h	90 (83)	97
 19a 19b-cis + trans isomer	6	{S-2}Hf	5 d	90	96
	7	{1}Zr	20 h	100 (2:1)	-
	8	{S-2}Zr	0.3 h	(95; 4:1)	97, 95
	9	{S-2}Zr	2 d	100 ^e (1:1.3)	99, 99 ^f
 10a 10b-cis + trans isomer	10	{S-2}Hf	3 h	(84; 2:1)	93, 96
	11	{S-3}Zr	48 h	100 (1:1.2)	96, 98
	12	{1}Zr	30 h	85, (1.5:1)	-
 13a 13b-cis + trans isomer	13	{S-2}Zr	0.5 h	(90; 1:1)	93, 92
	14	{S-2}Hf	20 h	(81; 1.4:1)	87, 63
	15	{S-3}Zr	30 h	85 (1.2:1)	92, 91
 16a 16b	16	{1}Zr	4 d	20	-
	17	{S-2}Zr	4 d	85 (77)	89
 18a 18b	18	{1}Zr	20	95 (1.4:1)	-
	19	{S-2}Zr	15	(89; 3:1)	66, 57
	20	{S-2}Hf	24	90 (2.5:1)	65, 58

^aReaction conditions: 10 mol % catalyst, room temperature. ^bIsolated yield is given in parentheses. ^cRatio of diastereomers defined as *cis/trans*. ^dPercent enantiomeric excess ($\pm 0.5\%$) was determined by ¹⁹F NMR spectra of Mosher amide derivatives. ^eAt -30 °C. ^fPercent enantiomeric excess verified by HPLC.

$2\}\text{Zr}(\text{NMe}_2)_2 > \{1\}\text{Zr}(\text{NMe}_2)_2 > \{S-3\}\text{Zr}(\text{NMe}_2)_2$. For example, the diphenyl substrate **8a** is cyclized to 4,4-diphenyl-2-methylpyrrolidine **8b** in 1.25 h by $\{S-2\}\text{Zr}(\text{NMe}_2)_2$, 11 h by $\{1\}\text{Zr}(\text{NMe}_2)_2$, and 18 h by $\{S-3\}\text{Zr}(\text{NMe}_2)_2$ (Table 3, entries 2, 1, and 9). This trend applies to the formation of most pyrrolidine, azepane, and indoline products found in Tables 3–5. However, achiral $\{1\}\text{Zr}(\text{NMe}_2)_2$ provides a more active catalyst than $\{S-2\}\text{Zr}(\text{NMe}_2)_2$ for the unsubstituted amino-pentene **13a** (Table 3, entries 29 and 30) and aminohexenes **14a** and **15a** (Table 4, entries 1 and 2). Substrate **13a** is readily cyclized by $\{1\}\text{Zr}(\text{NMe}_2)_2$ even at room temperature, while $\{S-2\}\text{Zr}(\text{NMe}_2)_2$ requires 110 °C for only a few turnovers. Only **13a** and HNMe_2 are detected with $\{S-2\}\text{Hf}(\text{NMe}_2)_2$, $\{S-2\}\text{Ti}(\text{NMe}_2)_2$, or $\{S-3\}\text{Zr}(\text{NMe}_2)_2$ as precatalysts.

Several generalizations about the influence of ancillary ligand, metal center, solvent, and temperature on enantioselectivity are apparent. Overall, this group 4 system provides pyrrolidines with excellent optical purities. For example, **8a** is cyclized to *R*-**8b** with 98% ee in the presence of $\{S-2\}\text{Zr}(\text{NMe}_2)_2$ at -30 °C and in 97% ee with $\{S-2\}\text{Hf}(\text{NMe}_2)_2$ at 0 °C (Table 3, entries 5 and 7). Impressively, the enantioselectivities of reactions catalyzed by $\{S-2\}\text{Zr}(\text{NMe}_2)_2$ are high for a range of aminoalkenes. In the series of pyrrolidines, spirocyclohexyl **12b** (90%), spirocyclopentyl **9b** (92%), trimethyl **10b** (89%), and diallyl **11b** (93%) are obtained with high enantiopurity at room temperature using $\{S-2\}\text{Zr}(\text{NMe}_2)_2$ (Table 3). The enantioselectivity is not sensitive to catalyst loading. For example, 2–15 mol % of $\{S-2\}\text{Zr}(\text{NMe}_2)_2$ provides **8b** with 93% ee at all catalyst loadings.

In general, $\{S-2\}\text{Zr}(\text{NMe}_2)_2$, $\{S-2\}\text{Hf}(\text{NMe}_2)_2$, and $\{S-3\}\text{Zr}(\text{NMe}_2)_2$ provide products with better optical purities than the titanium-based precatalyst $\{S-2\}\text{Ti}(\text{NMe}_2)_2$. The isopropyl-5,5-dimethyl-2-oxazoline ligands often give pyrrolidines with higher % enantiomeric excesses than the 4*S*-*tert*-butyl-2-oxazoline ligand. In contrast, the trivalent yttrium catalyst system containing the 4*S*-*tert*-butyl-2-oxazoline-based ligand provides pyrrolidines with higher % ee than $\{S-2\}\text{YCH}_2\text{SiMe}_3$.¹¹ In the present zirconium system, tri(allyl)methylamine **11a** is cyclized with $\{S-2\}\text{Zr}(\text{NMe}_2)_2$ to give 4,4-diallyl-2-methylpyrrolidine **11b** with 93% ee, whereas the enantioselectivity provided by $\{S-3\}\text{Zr}(\text{NMe}_2)_2$ is 88%. Similar effects are observed with the cyclopentyl substrate (92% vs 88%) and cyclohexyl substrate (90% vs 87%), while the diphenyl pyrrolidine forms with equivalent % ee using $\{S-2\}\text{Zr}(\text{NMe}_2)_2$ and $\{S-3\}\text{Zr}(\text{NMe}_2)_2$. As expected, the mirror-image precatalyst $\{R-2\}\text{Zr}(\text{NMe}_2)_2$ gives equivalent reactivity and enantioselectivity as $\{S-2\}\text{Zr}(\text{NMe}_2)_2$ but provides the products with the opposite absolute configuration (eq 9). Thus, an additional advantage of the valine-derived ligands versus *tert*-leucine is that both enantiomers are readily available for the former.



The hafnium precatalyst $\{S-2\}\text{Hf}(\text{NMe}_2)_2$ is also highly enantioselective, and the examples here are the first in which a hafnium complex affords hydroamination products with optical

purities >90%. In fact, $\{S-2\}Hf(NMe_2)_2$ provides pyrrolidines with higher enantioselectivity than $\{S-2\}Zr(NMe_2)_2$ (under equivalent conditions) for about half of the aminoalkenes that were tested. In particular, $\{S-2\}Hf(NMe_2)_2$ gives higher % ee in benzene- d_6 at room temperature for cyclopentylpyrrolidine (**9b**, 95% ee) and cyclohexylpyrrolidine (**12b**, 93% ee). However, under these conditions, 4,4-diphenyl (**8b**), 4,4-dimethyl (**10b**), and 4,4-diallyl-2-methylpyrrolidine (**11b**) are formed with greater optical purities in reactions catalyzed by $\{S-2\}Zr(NMe_2)_2$ than $\{S-2\}Hf(NMe_2)_2$. The enantiomeric excesses were always lowest with $\{S-2\}Ti(NMe_2)_2$ as the precatalyst, regardless of the substrate. Thus, the effect of metal center on enantioselectivity follows the trend $Zr \approx Hf > Ti$ for this mixed cyclopentadienylbis(oxazolinyl)borate group 4 system.

High optical purities are obtained from reactions performed in benzene, toluene, methylene chloride, and THF. However, the apparent turnover rate is diminished in THF and methylene chloride compared to benzene and toluene. With the $\{S-2\}Zr(NMe_2)_2$ -catalyzed cyclization of **8a** as a representative example, benzene- d_6 and methylene chloride- d_2 solvents provide the same enantioselectivity (93% ee), although the reaction is faster in benzene- d_6 . Higher enantiomeric excess is obtained in THF at room temperature (95%, Table 3, entry 3), and conditions of lower temperature ($-30^\circ C$) in toluene- d_8 solvent provide the product with 98% ee.

In fact, the asymmetric induction is significantly enhanced at lower temperatures, although long reaction times are needed in several cases. For example, $\{S-2\}Zr(NMe_2)_2$ catalyzes the formation of 2,4,4-trimethylpyrrolidine **10b** at $-30^\circ C$ with 93% enantiomeric excess, whereas the product is formed with 89% ee at room temperature (Table 3, entries 16 and 17). A similar trend is also observed for $\{S-2\}Hf(NMe_2)_2$, which mediates the formation of 4,4-diallyl-2-methylpyrrolidine **11b** with 96% ee at $0^\circ C$ (Table 3, entry 21) compared to 90% ee at room temperature.

Thus, $\{S-2\}Zr(NMe_2)_2$ provides a highly effective catalyst for the asymmetric cyclization of aminoalkenes to 2-methylpyrrolidines. Typically, hydroaminations of aminohexenes and aminoheptenes (Table 4) are more difficult than the aminopentenes of Table 3. In fact, the rates of conversion of aminohexenes **14a** and **15a**, as catalyzed by $\{S-2\}Zr(NMe_2)_2$, are significantly decreased with respect to the aminopentenes. Additionally, the enantiomeric excesses of the 2-methylpiperidine products are significantly lower than the 2-methylpyrrolidines. The catalytic rate of $\{S-2\}Hf(NMe_2)_2$ is superior to the rate of the zirconium congener for piperidine formation, although elevated temperature is required.

The cyclization of an aminoheptene substrate is catalyzed by $\{1\}Zr(NMe_2)_2$ to give a racemic azapane and by $\{S-2\}Zr(NMe_2)_2$ to provide the product in highly optically enriched form (Table 4, entries 8 and 9). However, the hafnium and titanium complexes $\{S-2\}Hf(NMe_2)_2$ and $\{S-2\}Ti(NMe_2)_2$, as well as the *tert*-butyl-oxazolinylborate zirconium complex $\{S-3\}Zr(NMe_2)_2$, are not effective even at elevated temperatures.

The high enantioselectivity in aminopentene cyclizations motivated further study of five-membered nitrogen-containing ring formations. The catalysts obtained from $\{S-2\}Zr(NMe_2)_2$ and $\{S-2\}Hf(NMe_2)_2$ cyclize *ortho*-allylaniline (**17a**) at room temperature to generate optically active 2-methylindoline (**17b**) with 95 and 94% ee, respectively (Table 5, entries 2 and 3). 2-Substituted indolines are important subunits in cannabinoid receptor agonists, as well as in drug candidates

including eletriptan and indapamide.⁴⁸ Previously described syntheses of highly enantioenriched (>90%) 2-stereogenic indolines rely on either catalytic asymmetric hydrogenation of indoles or kinetic resolution of racemic indolines.^{49,50} Previously reported hydroamination catalysts provide 2-methylindoline from *ortho*-allylaniline with moderate enantioselectivity.^{15,22} Therefore, complexes $\{S-2\}Zr(NMe_2)_2$ and $\{S-2\}Hf(NMe_2)_2$ are promising for preparation of optically active indoline building blocks from aniline derivatives.

Hydroaminations in methylene chloride and THF, described above, hint at functional group tolerance. Therefore, we investigated cyclization reactions of aminopentenes that contain halogen or ether functionality. Quite promisingly, high enantiomeric excess is obtained in the conversion of 2,2-diethoxyaminopentene **18a** catalyzed by $\{S-2\}Zr(NMe_2)_2$ (97% ee) and $\{S-2\}Hf(NMe_2)_2$ (96% ee; Table 5, entries 5 and 6). The achiral $\{1\}Zr(NMe_2)_2$ mediates the cyclization at approximately the same rate as $\{S-2\}Zr(NMe_2)_2$, but neither the 4*S*-*tert*-butyl-oxazolinylborate-based $\{S-3\}Zr(NMe_2)_2$ nor titanium-based compounds are effective.

2-Allyl-2-(4-bromophenyl)pent-4-enylamine **19a** is cyclized by $\{1\}Zr(NMe_2)_2$ to a 2:1 diastereomeric mixture of *cis*- and *trans*-pyrrolidines at room temperature (Table 5, entry 7). The assignment of the major isomer as *cis* is supported by NOE experiments in benzene- d_6 in which irradiation of the 2-methyl signal of the major isomer (1.00 ppm) gives decreased intensity of the *ortho*- and *meta*-phenyl resonances at 7.27 and 6.69 ppm for that isomer. Interestingly, the optically active $\{S-2\}Zr(NMe_2)_2$ is more efficient (full conversion in 20 min) than the achiral catalyst, gives better diastereoselectivity (*cis/trans* = 4:1), and provides the products with exceedingly high enantioselectivity for both diastereomers (*cis*, 97% ee; *trans*, 95% ee). The diastereomeric ratio (*cis/trans* = 2:1) and the optical purity of the major enantiomer (at 93% ee) are lower with $\{S-2\}Hf(NMe_2)_2$. High optical purity is obtained with $\{S-3\}Zr(NMe_2)_2$ (Table 5, entry 11), although the diastereomeric ratio is 1:1.2 (but now favoring the *trans* isomer) and the reaction time is 2 days. Finally and impressively, both diastereomers are obtained in 99% ee after cyclization at $-30^\circ C$ in toluene with $\{S-2\}Zr(NMe_2)_2$. However, at that temperature, the diastereoselectivity decreased to 1:1.3 (with the *trans* isomer slightly favored).

In the cyclization of 4-aminomethyl-4-methylhepta-1,6-diene (**20a**), the fastest cyclization rate is obtained with $\{S-2\}Zr(NMe_2)_2$ and the greatest diastereoselectivity is obtained with $\{1\}Zr(NMe_2)_2$. However, the diastereomeric ratio obtained with substrate **20b** is generally lower than with **19b**.

Cyclization of the amino 1,2-disubstituted alkene **21a** to **21b** is mediated by $\{1\}Zr(NMe_2)_2$ and $\{S-2\}Zr(NMe_2)_2$ (89% ee). However, $\{S-2\}Hf(NMe_2)_2$, $\{S-2\}Ti(NMe_2)_2$, and $\{S-3\}Zr(NMe_2)_2$ are not effective at room or elevated temperatures.

Throughout, we have seen that the turnover rate diminishes with decreasing steric bulk in the 3,3-position of the aminopentenes, following the often-invoked *gem*-disubstitution effect.^{5,51} As noted above, the parent aminopentene is not efficiently cyclized by any of these chiral oxazolinylborate catalysts. Accordingly, the rate of cyclization of 2-phenylpent-4-en-1-amine **22a** is decreased significantly compare to the diphenylaminopentene **8a**. Furthermore, the optical purity decreases substantially for both diastereomers.

4. Spectroscopic and Kinetics Features of Catalytic Reactions. The olefin hydroamination reactions catalyzed by $\{S-2\}Zr(NMe_2)_2$ are unique among group 4 systems in terms of

the mild conditions of conversion (room temperature to -30 °C), the broadly high enantioselectivity, and the relative insensitivity of the enantioselectivity to solvent choice. We have collected additional data to characterize some of the kinetic and stereochemical features of our system to rule out possible catalytic pathways and possibly identify the features that provide high rates and high enantioselectivity. We have also investigated effects of ancillary ligand modifications on cyclization rates that, along with the kinetic data, provide a mechanistic hypothesis that best explains the currently available data.

4.1. Reaction Time Course and Its Kinetic Features.

HNMe₂ is observed by ¹H NMR spectroscopy upon addition of the aminoalkenes to the precatalyst. The resting state of the catalyst is not readily assigned from ¹H NMR spectra of micromolar reactions performed in deuterated solvents. However, the active species is formed at room temperature within 1 min, based on the appearance of product in the ¹H NMR spectrum of the reaction mixture.

A ¹H NMR spectrum of the reaction of 1 equiv of C-(1-allyl-cyclohexyl)methylamine (**12a**) and {S-2}Zr(NMe₂)₂ at 230 K in toluene-*d*₈ contained resonances assigned to HNMe₂ (2.20 ppm) and new olefin moieties (5.81 and 5.10 ppm) associated with transformation of **12a** but not its cyclization. In addition, resonances assigned to the ancillary ligand and ZrNMe₂ were detected. Peaks from **12a** and the {S-2}Zr(NMe₂)₂ starting material are not visible in this mixture. For comparison, the ¹H NMR spectrum of **12a** at 230 K contained olefinic resonances at 5.69 and 4.99 ppm. Aminopentene **12a** cyclizes upon warming to room temperature. The final spectrum after 12 h contained signals from HNMe₂ and a mixture of resonances tentatively assigned as the two diastereomers of {S-2}Zr(**12b**-H)(NMe₂).

A ¹H NMR spectrum of the reaction of {S-2}Zr(NMe₂)₂ and 2 equiv of **12a**, mixed, maintained, and acquired at 230 K, contained signals assigned to HNMe₂. The ¹H NMR signals previously assigned to ZrNMe₂ and **12a** were absent from the spectrum. However, the ¹H NMR spectrum of the reaction mixture was complicated by broad overlapping resonances in the phenyl and cyclopentadienyl regions, and structural assignment was not possible. Similarly, broad resonances for {S-2}Zr-species were observed in catalytic reaction mixtures at low temperature; therefore, assignment of the structure of a catalytic resting state is not possible at this point.

Instead, the reaction pathway was characterized using kinetic studies. The concentrations of the “cyclohexyl” substrate **12a** and the cyclized spiro product **12b** were monitored by ¹H NMR spectroscopy over the course of the catalytic conversion. Plots of ln[**12a**] versus time are linear (up to 75–82% conversion, Figure 4), and this is consistent with first-order dependence on substrate concentration. Using the first 75% of the reaction, a series of pseudo-first-order rate constants (*k*_{obs}) are obtained for a range of initial concentrations of {S-2}Zr(NMe₂)₂. A linear relationship between *k*_{obs} and [{S-2}Zr(NMe₂)₂] provides the empirical rate law: $-d[12a]/dt = k'_{obs}[12a][\{S-2\}Zr(NMe_2)_2]^1$ (*k*'_{obs} = 0.128 ± 0.007 M⁻¹ s⁻¹; 21 °C).⁵²

However, after two half-lives, the reaction rate decreases to a greater degree than expected for a first-order reaction. Similar observations have been reported in other early metal-catalyzed amino-olefin cyclizations (although typically these showed zero-order substrate concentration dependence), and the nonlinearity was attributed to product inhibition.^{53,54} Recently,

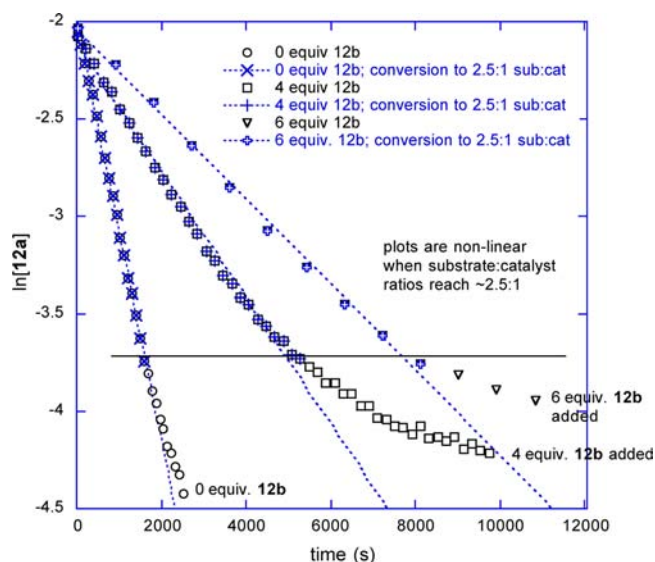


Figure 4. Plots of ln[**12a**] versus time for the {S-2}Zr(NMe₂)₂-catalyzed conversion of **12a** into pyrrolidine **12b**. Three experiments are illustrated, in which [{S-2}Zr(NMe₂)₂] = 9.7 mM and 0, 4, and 6 equiv of the product **12b** is added prior to conversion. Linear least-squares best fits for ~2.5 half-lives corresponds to conversion to substrate/Zr molar ratio = 2.5:1 for the three data sets.

Schafer pointed out that the curvature might result from a change in rate law rather than product blocking catalytic sites.³¹ We therefore pursued this point by measuring rates and determining the rate laws in the presence of product. Cyclization rates of **12a** catalyzed by {S-2}Zr(NMe₂)₂ were measured with 4 and 6 equiv of product **12b** (using 90% ee material) relative to catalyst, and pseudo-first-order rate constants (0 equiv of **12b**, *k*_{obs} = 1.08 × 10⁻³ s⁻¹; 4 equiv of **12b**, *k*_{obs} = 0.32 × 10⁻³ s⁻¹; 6 equiv **12b**, *k*_{obs} = 0.22 × 10⁻³ s⁻¹) were smaller in the presence of **12b** (measured with equivalent catalyst concentration {S-2}Zr(NMe₂)₂). Thus, kinetic experiments indicate that addition of product results in slower conversion (without a change in rate law) consistent with product inhibition.

Interestingly, even in the presence of 6 equiv of **12b**, plots of ln[**12a**] versus time are linear only up to ~75% conversion. In general, the ln[**12a**] versus time plots deviate from first-order substrate dependence at a ratio of [substrate]/[catalyst] ~ 2.5. This apparent effect may be related to the requirement that two molecules of **12a** are needed for catalytic turnover (see the initial rates experiments below). Thus, these experiments suggest that the curvature in first-order plots results from a change in mechanism at low substrate concentration in addition to the effects of high product concentration. These effects should be minimized under conditions of high [**12a**].

An additional observable that can provide insight into possible mechanism change is the enantioselectivity, which will be sensitive to catalyst structure. Therefore, the % ee was monitored as a function of conversion (Figure 5). Notably, this plot shows that the % ee is constant from 35 to 70% conversion, and the enantioselectivity begins to decrease above 75% conversion. Furthermore, the lower enantioselectivity occurs at the same % conversion at which the rate appears to deviate from first-order. However, the observed % ee is invariant over experiments in which the absolute concentration of the reaction mixture is varied. Furthermore, experiments in which **12b** product is added prior to catalysis provide the total

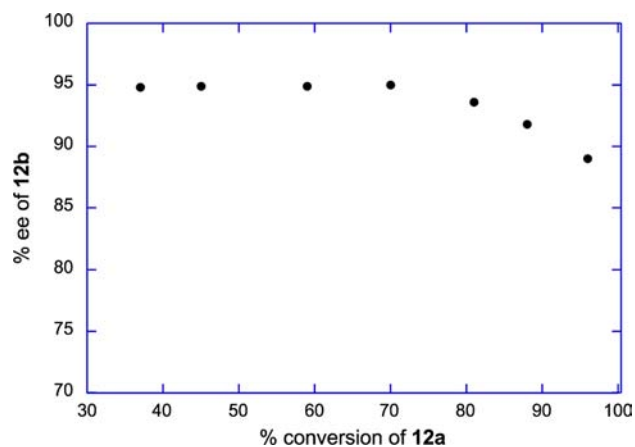


Figure 5. Plot showing the correlation of enantiomeric excess of pyrrolidine product **12b** with catalytic conversion of substrate **12a**.

product with identical optical purity (i.e., the product is not influencing the enantioselectivity).

Mechanistic studies of early transition-metal, lanthanide-, and actinide-catalyzed hydroamination/cyclization have probed the kinetic features (isotope effects, temperature dependence) based on some percentage of catalytic conversion due to apparent product inhibition. Based on those precedents, the kinetic analysis here is performed using ~ 2.5 half-lives of data. Conversion of *C*-(1-allylcyclohexyl)methylamine-ND₂ (**12a-d₂**), catalyzed by {*S*-2}Zr(NMe₂)₂, is much slower than conversion **12a** itself. The second-order rate constant $k'_{\text{obs}}^{(\text{D})}$ ($0.039 \pm 0.002 \text{ M}^{-1} \text{ s}^{-1}$) and the large $k'_{\text{obs}}^{(\text{H})}/k'_{\text{obs}}^{(\text{D})}$ value (3.3 ± 0.2) is consistent with a primary isotope effect (i.e., a N–H or N–D bond is broken in the transition state of the turnover-limiting step). In addition, second-order rate constants (k'_{obs}) for cyclization of **12a** were measured at temperatures from 266 to 314 K. The plot of $\ln(k'_{\text{obs}}/T)$ versus $1/T$ from these data provides the values of activation parameters: $\Delta H^\ddagger = 11.0(6) \text{ kcal}\cdot\text{mol}^{-1}$ and $\Delta S^\ddagger = -24(2) \text{ cal}\cdot\text{mol}^{-1} \text{ K}^{-1}$.

4.2. Initial Rates. The potential simplification of kinetic studies at high [**12a**] and low [**12b**] motivated investigations of the instantaneous rate dependence on substrate concentration for the first 8–20% of the catalytic conversion (corresponding to ~ 2 catalytic turnovers). At low concentrations (0.0098 to 0.07 M), the average initial substrate conversion rates increase linearly as the substrate concentration increases; however, at higher substrate concentrations (70 mM), the initial rates reach a maximum. A slight decrease of the initial rate is observed at [**12a**] > 70 mM. Plots of initial rates versus substrate concentration thus show saturation in substrate concentration (Figure 6), and experiments that probe initial rate dependence on substrate concentration performed at 273, 314, and 322 K, as well as using N-deuterated substrate **12a-d₂**, provide similar curves. As can be seen in Figure 6, the initial rate plots also contains a nonzero x -intercept that coincides with catalyst concentration. This nonzero intercept suggests that 1 equiv of substrate is required before one catalytic cycle can be completed. That statement is an approximation, in fact, because the low-temperature experiments with 1:1 substrate to catalyst ratio indicate that cyclization can occur at that low ratio (presumably resulting from formation of a mixture that contains {*S*-2}Zr(**12a-H**)₂). However, as suggested by the

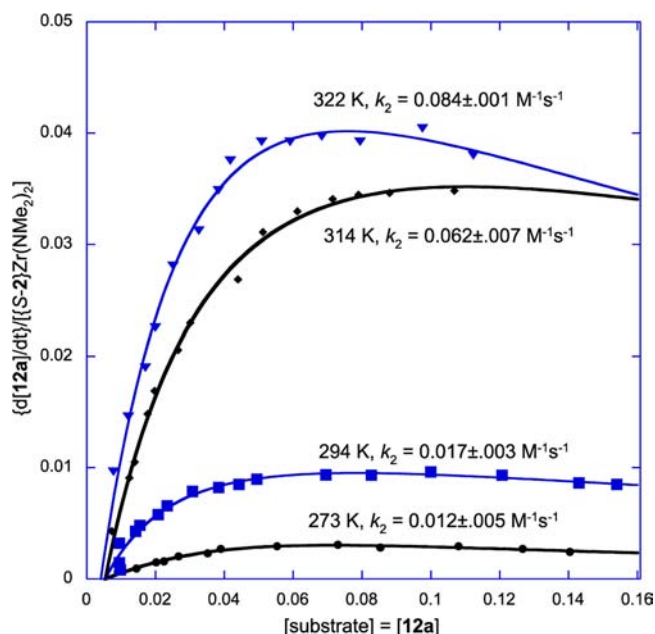


Figure 6. Plots of initial rates of cyclization $-d[\mathbf{12a}]/dt$ versus $[\mathbf{12a}]_{\text{ave}}$ for cyclization of **12a** at 273, 294, 314, and 322 K. The curves represent nonlinear least-squares regression analysis of the data to the equation $-d[\mathbf{12a}]/dt = k_2[\text{Zr}][\mathbf{12a}]/\{K' + [\mathbf{12a}] + K_{\text{SI}}[\mathbf{12a}]^2\}$.

$\ln[\text{substrate}]$ versus time plots, the reaction rate drops precipitously at low substrate concentrations.

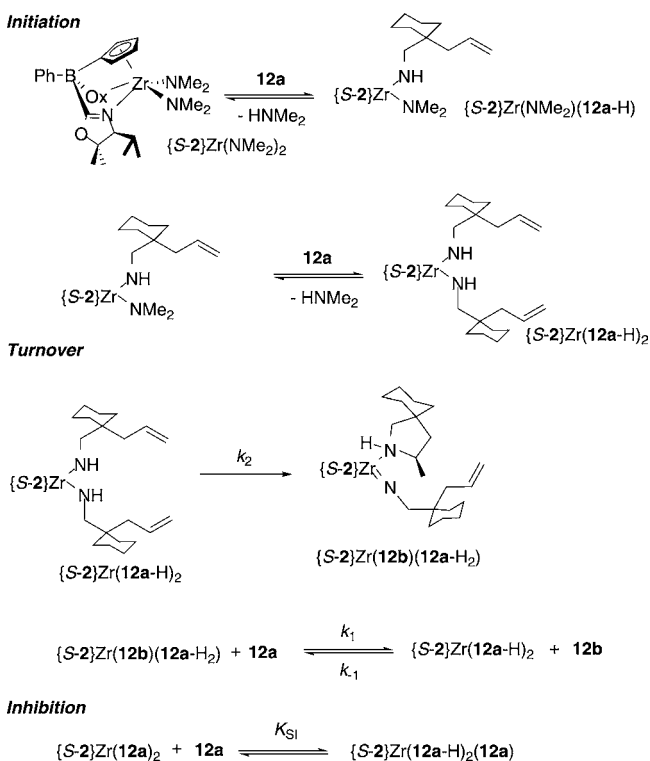
The nonlinear rate dependence on concentration indicates that the rates of the elementary reaction steps are inequivalently influenced by substrate concentration; the result is that changing substrate concentration modifies the contribution of the elementary steps to the rate of catalysis. Nonlinear least-squares regression analysis of the data in Figure 6 provides good correlation with eq 10, which includes the rate constant k_2 for the irreversible step, the catalyst formation constant K' ($\{k_{-1} + k_2\}/k_1$), and the substrate inhibition constant K_{SI} . The form of the rate equation resembles the Michaelis–Menten equation, with the addition of a reversible substrate inhibition step (eq 11).⁵⁵ Additionally, the substrate concentration in eq 11 is modified by the approximated requirement that 1 equiv of substrate **12a** is needed to convert {*S*-2}Zr(NMe₂)₂ precatalyst into an active form of the catalyst, giving the terms $\{[\mathbf{12a}] - [\{\text{S-2}\}\text{Zr}(\text{NMe}_2)_2]\}$ in eq 10.

$$\frac{-d[\mathbf{12a}]}{dt} = \frac{k_2[\{\text{S-2}\}\text{Zr}(\text{NMe}_2)_2]\{[\mathbf{12a}] - [\{\text{S-2}\}\text{Zr}(\text{NMe}_2)_2]\}}{(K' + \{[\mathbf{12a}] - [\{\text{S-2}\}\text{Zr}(\text{NMe}_2)_2]\} + K_{\text{SI}}\{[\mathbf{12a}] - [\{\text{S-2}\}\text{Zr}(\text{NMe}_2)_2]\}^2)} \quad (10)$$

$$\frac{-d[\text{substrate}]}{dt} = \frac{(k_2[\text{catalyst}][\text{substrate}])}{\left(\frac{k_{-1} + k_2}{k_1} + [\text{substrate}] + K_{\text{SI}}[\text{substrate}]^2\right)} \quad (11)$$

The three parameters obtained from the curve fit are k_2 ($1.7 \pm 0.3 \times 10^{-2} \text{ s}^{-1}$), K' ($2.8 \pm 0.7 \times 10^{-2} \text{ M}$), and K_{SI} ($5 \pm 2 \text{ M}^{-1}$). The rate law in eq 10 corresponds to the reaction mechanism shown in Scheme 4, which shows reversible substrate and catalyst association followed by an irreversible step. This rate

Scheme 4. Hydroamination Mechanism Based on Interpretation of [12a] versus Initial Rate Plots



law and the observations given above provide a rudimentary reaction pathway for which some rate constants are known and the speciation of some intermediates can be surmised. The isotope effect for conversion $k'_{\text{obs}}(\text{H})/k'_{\text{obs}}(\text{D})$ could thus result from an equilibrium isotope effect $K'(\text{H})/K'(\text{D})$, a kinetic isotope effect $k_2(\text{H})/k_2(\text{D})$, or a combination of both.

Room temperature kinetic investigations provide an equilibrium isotope effect (for the formation constant K') of 1.9 ± 0.5 . The kinetic isotope effect that employs the turnover-limiting rate constant k_2 is 2.3 ± 0.4 .

In order to evaluate the transition state features of the irreversible step, experiments that probe the effect of temperature on initial rate versus [12a] were pursued. From the nonlinear least-squares best fits, k_2 values were determined for catalysis at temperatures of 273, 294, 314, and 322 K. Using the Eyring equation, the plot of $\ln(k_2/T)$ versus $1/T$ provides $\Delta H^\ddagger = 6.7(2)$ kcal·mol⁻¹ and $\Delta S^\ddagger = -43(7)$ cal·mol⁻¹ K⁻¹. Notably, the “saturation kinetics” show a highly organized transition state and low activation enthalpy. The values from the initial rate analysis are not equal to the values obtained from conversion kinetics described above, and this reflects k'_{obs} as a combination of more than one elementary step.

Cyclization reactions of *N*-deutero-aminoalkenes give 2-methylpyrrolidines and a 2-methylpiperidine with higher enantiomeric excesses than the corresponding proteo-aminoalkene. As shown in Table 6, the % ee values for deuterio-heterocycles are higher compared to the corresponding proteo-heterocycles with the {S-2}Zr(NMe₂)₂. Using this method, the % ee can be enhanced from 90 to 97% under otherwise identical reaction conditions! Interestingly, even the piperidine formations that proceed with lower enantioselectivity show the same trend. Similarly, the {S-2}Hf(NMe₂)₂ and {S-3}Zr(NMe₂)₂ compounds provide deuterio-heterocyclic products

Table 6. Effect of *N*-d₂ Substitution on % ee in Enantioselective Hydroamination^a

product	{S-2}Zr	{R-2}Zr	{S-2}Hf	{S-3}Zr
8b	93 (R)	93 (S)	91 (R)	93 (R)
8b-d ₂	95 (R) 97 (R) ^b	95 (S)	96 (R)	96 (R)
12b	90 (R)	90 (S)	93 (R)	86 (R)
12b-d ₂	97 (R) 98 (R) ^c	97 (S)	97 (R)	91 (R)
14b	31 (R)	31 (S)	26 (R)	-
14b-d ₂	46 (R)	46 (S)	44 (R)	-

^aReaction conditions: 23 °C, C₆D₆, >95% yield. ^bAt 0 °C in toluene or THF. ^cAt -30 °C in THF.

with higher optical purities compared to the corresponding proteo-heterocycles. Thus, this stereochemical isotope effect is systemic, at least within this cyclopentadienylbis(oxazolinyl)-borato group 4 family of catalysts.

DISCUSSION

Catalyst Structure. Cyclopentadienylbis(oxazolinyl)-borato-supported group 4 diamide compounds are exceptionally active for cyclization of aminopentenes. Within the ligand class, variation of 4- and 5-substitution on the oxazoline affects complex stability, reaction rate in catalytic hydroaminations, and enantioselectivity. Achiral {1}Zr(NMe₂)₂ is more active for cyclization of the aminohexenes and the unsubstituted aminopentene, while {S-2}Zr(NMe₂)₂ is much more active for 3,3-disubstituted aminopentenes.

These effects warrant discussion of the coordination properties of the oxazoline groups. X-ray crystal structures of {1}Zr(NMe₂)₂ and {1}Zr(NMe₂)₂THF show that a single oxazoline is coordinated to zirconium. Low-temperature ¹H NMR spectroscopy indicated fluxionality in {1}Zr(NMe₂)₂THF, and IR studies showed two oxazoline bands. In contrast, the ¹H NMR spectrum of THF-free {1}Zr(NMe₂)₂ is invariant over a large temperature range, and the IR spectrum of amorphous material contained one oxazoline stretch. The IR spectrum of crystalline material, however, was consistent with the X-ray analysis. The coordination of {1}, {S-2}, and {S-3} under catalytic conditions could not be discerned from ¹H NMR spectra of reaction mixtures, even at low temperature.

Therefore, a mono(oxazolinyl)diphenylborate ligand H[S-7] and its zirconium complex {S-7}Zr(NMe₂)₂ were prepared (eq 8). The zirconium diamide is isolable and fully characterized. Mixtures of {S-7}Zr(NMe₂)₂ and aminopentenes 8a or 12a contained resonances associated with HNMe₂, the {S-7} ligand bonded to zirconium, and aminopentene. The expected pyrrolidine product is not detected. Even after 4 days at room temperature or heating at 140 °C for 2 days, the 2-methylpyrrolidine is not detected in the ¹H NMR spectra. We conclude that two oxazoline groups are required for catalysis to occur, although the mechanistic role of the two oxazolines is not defined by this experiment. However, given the observed

NMe₂ substitution by **12a** without formation of **12b** product, it is likely that both oxazolines are involved in the C–N/C–H bond formation step.

The cyclopentadienylborate ligand occupies two valent sites of tetravalent zirconium, leaving two active amides. The reactivity of {S-2}Zr(NMe₂)Cl in aminopentene cyclizations was therefore explored to identify the importance of two active sites. In fact, aminopentenes are unchanged in the presence of catalytic amounts of {S-2}Zr(NMe₂)Cl. Although {S-2}Zr(NMe₂)Cl and **8a** react to give HNMe₂, pyrrolidine is not observed in the reaction mixture. The {S-2}-related resonances are broad, and the zirconium-containing product is not characterized. The lack of activity for this zirconium monoamido chloride complex is remarkable in comparison to the related constrained geometry (CG = Me₂Si(C₅Me₄)N*t*-Bu) system,²⁵ in which the mixed {CG}Zr(NMe₂)Cl is more reactive than the corresponding diamide complex for cyclizations.

Characterization of the Reaction Pathway. Mixtures of secondary *N*-methylaminoalkene **8a-Me** and {S-2}Zr(NMe₂)₂ results in substitution of the dimethylamide groups. Thus, HNMe₂ and a new species assigned as diamido {S-2}Zr(**8a-Me**)₂ were observed by in situ ¹H NMR spectroscopic experiments. However, conversion to the *N*-Me-pyrrolidine was not observed at room temperature or upon heating to elevated temperatures. Interestingly, 25% conversion of **NMe-8a** to **NMe-8b** (ca. 2.5 catalyst turnovers) occurs upon addition of a catalytic amount of amylamine or propylamine (1–2 equiv vs catalyst). Additional quantities of amylamine and/or elevated temperatures provide equivalent catalytic conversion (25%). These results suggest that, under these conditions, the zirconium center is bonded to an amidoalkene ligand and a second amido that contains an NH group; both ligands are needed for C–N bond formation to occur.

Kinetic experiments and isotopic effects on stereochemistry further support this proposal. Specifically, the plots of initial rate versus substrate concentration, extrapolated to the zero value of initial rate, suggest that the concentration of aminoalkene substrate must be greater than catalyst concentration (although this observation is limited by the quality of low substrate concentration/rate data). Thus, the slower cyclization rates observed at high conversion are in part attributed to low concentrations of aminoalkene substrate and in part to inhibition by the secondary amine product.

The increased enantioselectivity obtained with *N*-deuterated substrates demonstrates that NH functionality is intimately involved in the stereochemistry-determining step. This stereochemical effect, along with the kinetic isotope effect on the turnover-limiting step obtained from initial rate kinetics, suggests that the elementary step described by *k*₂ is also the step in which the absolute configuration is established. These observations disfavor mechanisms involving olefin insertion into a zirconium–nitrogen bond (path A, Scheme 1) and [2*π* + 2*π*] cycloaddition of a zirconium imido (path B, Scheme 1). Here, we should note that reversible insertion (or 2*π* + 2*π* addition) followed by irreversible protonation, suggested for magnesium, yttrium, and zirconium catalyses from computational investigations,⁵⁶ is unlikely given the observations with {S-2}Zr(NMe₂)Cl as a precatalyst precursor and the need for a NH-containing amido ligand to be present in the turnover-limiting step. For the observed saturation kinetics to involve reversible insertion, reversible proton transfer prior to irreversible protonation is also required. If this were the case,

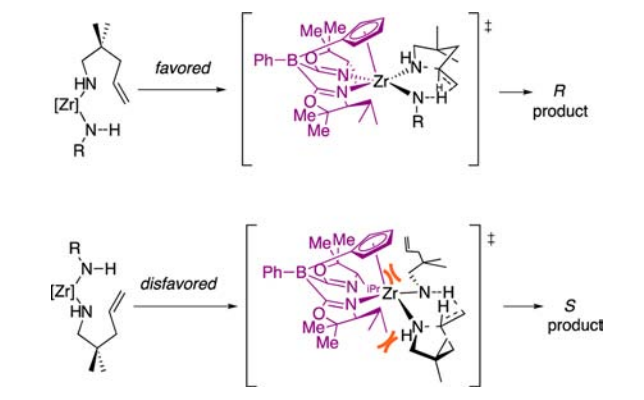
the enantioselectivity might be expected to be affected by the concentration of the substrate. While the % ee for the pyrrolidine product decreases at high conversion, the overall enantioselectivity is identical in experiments that systematically vary the overall reaction mixture concentration (as long as the comparison involves equivalent conversions). All of our kinetic evidence and chemical observations point to a conversion in which a zirconium center, an oxazolinyborate ancillary ligand, a “cyclizable” amidoalkene ligand, and a primary amide ligand are present in the turnover-limiting step. The pathway that best fits the data discussed above is described by path C of Scheme 1.

The nature of the proposed transition state in the turnover-limiting step of path C, then, is probed by activation parameters associated with the initial rate measurements and isotope effects on rate and stereochemistry. In particular, the ΔS^\ddagger for the turnover-limiting step is large and negative, indicating a highly ordered transition state; the activation enthalpy contributes only a small component of the overall barrier. Interestingly, the activation parameter values from conversion kinetics show more significant enthalpic contribution and a less significant entropic contribution to the overall barrier. The distinction between initial rate kinetics and conversion kinetics is important because the reversible step in the catalytic cycle is included in the *k*'_{obs} rate constant from the empirical rate law for conversion. Temperature-dependent equilibria thus impact and disguise the activation parameters that describe the irreversible step in the cycle. As a result, activation parameters associated with *k*'_{obs} provide an incorrect description of the transition state. Because the initial rate measurements provide the rate constant *k*₂ for the irreversible step (or at least the combination of elementary steps that summarize to *k*₂), the association of substrate and catalyst is separated from the irreversible step. That is, the highly negative ΔS^\ddagger in the initial rate kinetics describes a highly organized unimolecular transformation.

At the same time, the primary kinetic isotope effect shows N–H bond cleavage in the transition state. Additionally, the initial rate data (*k*₂^(H) and *k*₂^(D)) and the enantiomeric excess values for **12b** and **12b-d**₂ provide isotope effects for the diastereomeric pathways leading to the major and minor enantiomers. The kinetic isotope effect (*k*₂^(H)/*k*₂^(D) = 2.2(5)) that provides the major enantiomer is relatively small; however, the corresponding isotope effect for the minor pathway is significant (7.7(1)). Thus, the increase in enantioselectivity with **12a-d**₂ versus **12a** is a result of the minor pathway slowing to a greater extent than the major pathway. The larger isotope effect may suggest a more symmetrical proton transfer for the less favored pathway. Although specific interactions between the amidoalkene and the ancillary ligand {S-2} in the transition state cannot be probed directly by experiments, the relative positions of the two reactive amide sites with respect to {S-2} are suggested by NOESY experiments. The two sites are inequivalent by symmetry, and NOESY experiments also indicate that there are significantly dissimilar interactions between the amide groups and the oxazoline ligands. One amide is situated between two coordinated oxazolines, whereas the second amide group is located in the open space between one oxazoline and the cyclopentadienyl group. We speculate that cyclization of one of the amides is favored and leads to the *R* product, while cyclization from the other amide site provides the minor 2*S*-2-methylpyrrolidine (Scheme 5).

This idea is further supported by the effect of deuteration on the enantioselectivity. In particular, the isotope effect indicates

Scheme 5. Proposed Stereochemical Model



that the two diastereomeric transition states are dissimilar. Two sterically inequivalent sites provided by the C_1 -symmetric catalyst provide a reasonable mechanistic rationalization for generating sufficiently inequivalent shapes of the transition state.

A second consideration is the coordination geometry of the $\{S-2\}$ ligand during the catalytic cycle. The fluxionality of the ligands is enhanced under conditions of excess THF; furthermore, the $\{S-2\}Zr$ system is highly fluxional under catalytic conditions. An achiral model species, in which one oxazoline is dissociated and the THF is coordinated, was characterized by an X-ray crystallographic analysis. Despite these data, a few points favor a cyclization requirement of both oxazolines interacting with Zr. First, the mono-oxazoline compound $\{S-7\}Zr(NMe_2)_2$ reacts with substrates to give $HNMe_2$ and zirconium amido compounds, but pyrrolidine is not formed even under forcing conditions ($>140^\circ C$, 2 days). Because C–N and C–H bond formation (cyclization) is turnover-limiting and occurs from the diamide species, a reasonable supposition is that the second oxazoline in the $\{S-2\}$ Zr species is required for cyclization. Second, the enantioselectivity of the catalytic species is unaffected by changes in concentration of the substrate (until the final stages of the reaction, as discussed in the next paragraph and illustrated in Figure 5). The rate, however, is diminished at high substrate concentrations because of a substrate inhibition, suggesting that the zirconium species containing three substrate molecules (and presumably a dissociated oxazoline) is not active or considerably less active.

A third important consideration is the apparent change in mechanism at the late stages of the catalytic conversion. The observations of (slightly) lower % ee and slower than expected $-d[12a]/dt$ occur concurrently at greater than 75% conversion. These two observations may be correlated; the implication of correlated rate law and stereoselectivity deviations is that another mechanism, possibly involving an alternative speciation of the $\{S-2\}Zr$ -based catalyst, becomes more important at the substrate/catalyst ratio of $\sim 2:1$.

This effect is independent of “product inhibition” because the same rate law for the first $\sim 75\%$ conversion was measured with and without excess pyrrolidine. Furthermore, the final % ee values are identical in catalytic experiments with and in the absence of excess 2-methylpyrrolidine. Note that the catalytic conditions (that give 90% ee) and 2-methylpyrrolidine additive (90% ee) were matched so that the optical purity of the final product (which is a mixture of pyrrolidine produced in the catalysis and present as the additive) would be 90% unless the

catalyst–product interaction gives poorer enantioselectivity. There is, however, a product inhibition effect because addition of excess pyrrolidine (90% ee) and substrate to the catalytic reaction mixture gives a slower catalytic reaction.

Therefore, our current hypothesis is that cyclization at aminoalkene/catalyst ratios $>2:1$ follows the proposed highly selective pathway, whereas under conditions with less substrate, the pathway is less enantioselective. In principle, these alternative pathways could involve other elementary steps, including but not limited to those suggested in Scheme 1. An alternative, however, might involve a coordinated amine acting as the proton transfer agent through a similar six-centered transition state. Further support for competing pathways in hydroaminations will require insight into the evolution of the zirconium speciation during catalytic conversions. Currently, experimental NMR spectroscopic studies on this catalytic system have been limited by fluxionality under reaction conditions, and we are currently exploring new systems to obtain additional data. However, this idea could explain the substantial effects of conditions, substrate identity, and catalyst structure on enantioselectivity in d^0 and f^0d^0 metal-mediated hydroaminations that have caused difficulties in the hunt for broadly applicable enantioselective catalysts.

CONCLUSION

Cyclopentadienylbis(oxazolonyl)borate-supported zirconium and hafnium diamide compounds provide highly active and effective, enantioselective catalysts for hydroamination/cyclization of amino-olefins. These catalysts provide optically enriched pyrrolidines at synthetically useful levels, even in the presence of functional groups; furthermore, highly enantioenriched indoline and azepanes are accessible with these catalysts. Our survey of several aminoalkenes highlights some of the possibilities, as well as some of the limitations, associated with $\{S-2\}Zr(NMe_2)_2$ in hydroamination catalysis. However, minor modifications to the ancillary ligand significantly affect precatalyst stability, catalytic conversion rates, and stereoselectivity. These effects suggest that ligand modifications, centered around the modular oxazolonylborate platform, can further advance catalytic activity and selectivity.

ASSOCIATED CONTENT

Supporting Information

Synthetic, catalytic, and kinetics procedures, error analysis, tables with detailed yield and % ee data for all substrates, NMR and HPLC conditions and data for evaluating optical purity, configuration assignments. This material is available free of charge via the Internet at <http://pubs.acs.org>.

AUTHOR INFORMATION

Corresponding Author

sadow@iastate.edu

Notes

The authors declare no competing financial interest.

ACKNOWLEDGMENTS

Prof. M. Jeffries-EL is thanked for providing access to her HPLC, and Prof. A. Bakac is gratefully thanked for valuable suggestions regarding kinetics experiments. This research was supported by the U.S. Department of Energy, Office of Basic Energy Sciences, Division of Chemical Sciences, Geosciences, and Biosciences through the Ames Laboratory (Contract No.

DE-AC02-07CH11358). NMR measurements were performed on instruments supported by NSF (CRIF-0946687 and MRI-1040098). This research was also supported by an allocation of advanced computing resources provided by the National Science Foundation (A.D.S. and T.L.W.). The computations were performed on Kraken at the National Institute for Computational Sciences.

REFERENCES

- (1) (a) Nugent, T. C. *Chiral Amine Synthesis: Methods, Developments and Applications*; Wiley-VCH: Weinheim, Germany, 2010. (b) Ricci, A. *Modern Amination Methods*; Wiley-VCH: Weinheim, Germany, 2000. (c) King, A. G.; Meinwald, J. *Chem. Rev.* **1996**, *96*, 1105–1122.
- (2) (a) Togni, A.; Grützmacher, H. *Catalytic Heterofunctionalization: From Hydroamination to Hydrozirconation*; Wiley-VCH: Weinheim, Germany, 2001. (b) Hong, S.; Marks, T. J. *Acc. Chem. Res.* **2004**, *37*, 673–686. (c) Hultsch, K. C. *Adv. Synth. Catal.* **2005**, *347*, 367–391. (d) Müller, T. E.; Hultsch, K. C.; Yus, M.; Foubelo, F.; Tada, M. *Chem. Rev.* **2008**, *108*, 3795–3892.
- (3) (a) Gagne, M. R.; Brard, L.; Conticello, V. P.; Giardello, M. A.; Stern, C. L.; Marks, T. J. *Organometallics* **1992**, *11*, 2003–2005. (b) Giardello, M. A.; Conticello, V. P.; Brard, L.; Gagne, M. R.; Marks, T. J. *J. Am. Chem. Soc.* **1994**, *116*, 10241–10254. (c) Douglass, M. R.; Ogasawara, M.; Hong, S.; Metz, M. V.; Marks, T. J. *Organometallics* **2002**, *21*, 283–292. (d) Hong, S.; Tian, S.; Metz, M. V.; Marks, T. J. *J. Am. Chem. Soc.* **2003**, *125*, 14768–14783. (e) Ryu, J.-S.; Marks, T. J.; McDonald, F. E. *J. Org. Chem.* **2004**, *69*, 1038–1052. (f) Yu, X.; Marks, T. J. *Organometallics* **2007**, *26*, 365–376.
- (4) (a) O'Shaughnessy, P. N.; Scott, P. *Tetrahedron: Asymmetry* **2003**, *14*, 1979–1983. (b) O'Shaughnessy, P. N.; Knight, P. D.; Morton, C.; Gillespie, K. M.; Scott, P. *Chem. Commun.* **2003**, 1770–1771. (c) O'Shaughnessy, P. N.; Gillespie, K. M.; Knight, P. D.; Munslow, I. J.; Scott, P. *Dalton Trans.* **2004**, 2251–2256.
- (5) (a) Collin, J.; Daran, J.-C.; Schulz, E.; Trifonov, A. *Chem. Commun.* **2003**, 3048–3049. (b) Collin, J.; Daran, J.-C.; Jacquet, O.; Schulz, E.; Trifonov, A. *Chem.—Eur. J.* **2005**, *11*, 3455–3462. (c) Riegert, D.; Collin, J.; Meddour, A.; Schulz, E.; Trifonov, A. *J. Org. Chem.* **2006**, *71*, 2514–2517. (d) Riegert, D.; Collin, J.; Daran, J.-C.; Fillebeen, T.; Schulz, E.; Lyubov, D.; Fukin, G.; Trifonov, A. *Eur. J. Inorg. Chem.* **2007**, 1159–1168. (e) Aillaud, I.; Lyubov, D.; Collin, J.; Guillot, R.; Hannedouche, J.; Schulz, E.; Trifonov, A. *Organometallics* **2008**, *27*, 5929–5936. (f) Hannedouche, J.; Aillaud, I.; Collin, J.; Schulz, E.; Trifonov, A. *Chem. Commun.* **2008**, 3552–3554. (g) Aillaud, I.; Wright, K.; Collin, J.; Schulz, E.; Mazaleyra, J.-P. *Tetrahedron: Asymmetry* **2008**, *19*, 82–92. (h) Aillaud, I.; Collin, J.; Duhayon, C.; Guillot, R.; Lyubov, D.; Schulz, E.; Trifonov, A. *Chem.—Eur. J.* **2008**, *14*, 2189–2200. (i) Chapurina, Y.; Hannedouche, J.; Collin, J.; Guillot, R.; Schulz, E.; Trifonov, A. *Chem. Commun.* **2010**, 46, 6918–6920. (j) Aillaud, I.; Collin, J.; Hannedouche, J.; Schulz, E.; Trifonov, A. *Tetrahedron Lett.* **2010**, *51*, 4742–4745. (k) Chapurina, Y.; Ibrahim, H.; Guillot, R.; Kolodziej, E.; Collin, J.; Trifonov, A.; Schulz, E.; Hannedouche, J. *J. Org. Chem.* **2011**, *76*, 10163–10172. (l) Queffelec, C.; Boeda, F.; Pouilhès, A.; Meddour, A.; Kouklovsky, C.; Hannedouche, J.; Collin, J.; Schulz, E. *ChemCatChem* **2011**, *3*, 122–126.
- (6) (a) Gribkov, D. V.; Hultsch, K. C.; Hampel, F. *Chem.—Eur. J.* **2003**, *9*, 4796–4810. (b) Gribkov, D. V.; Hampel, F.; Hultsch, K. C. *Eur. J. Inorg. Chem.* **2004**, 4091–4101. (c) Gribkov, D. V.; Hultsch, K. C. *Chem. Commun.* **2004**, 730–731. (d) Gribkov, D. V.; Hultsch, K. C.; Hampel, F. *J. Am. Chem. Soc.* **2006**, *128*, 3748–3759. (e) Reznichenko, A. L.; Hampel, F.; Hultsch, K. C. *Chem.—Eur. J.* **2009**, *15*, 12819–12827. (f) Vitanova, D. V.; Hampel, F.; Hultsch, K. C. *J. Organomet. Chem.* **2007**, *692*, 4690–4701. (g) Reznichenko, A. L.; Nguyen, H. N.; Hultsch, K. C. *Angew. Chem., Int. Ed.* **2010**, *49*, 8984–8987.
- (7) Heck, R.; Schulz, E.; Collin, J.; Carpentier, J.-F. *J. Mol. Catal. A* **2007**, *268*, 163–168.
- (8) (a) Kim, J. Y.; Livinghouse, T. *Org. Lett.* **2005**, *7*, 1737–1739. (b) Kim, H.; Kim, Y. K.; Shim, J. H.; Kim, M.; Han, M.; Livinghouse, T.; Lee, P. H. *Adv. Synth. Catal.* **2006**, *348*, 2609–2618.
- (9) (a) Meyer, N.; Zulys, A.; Roesky, P. W. *Organometallics* **2006**, *25*, 4179–4182. (b) Benndorf, P.; Jenter, J.; Zielke, L.; Roesky, P. W. *Chem. Commun.* **2011**, 47, 2574–2576.
- (10) (a) Xiang, L.; Wang, Q.; Song, H.; Zi, G. *Organometallics* **2007**, *26*, 5323–5329. (b) Wang, Q.; Xiang, L.; Song, H.; Zi, G. *Inorg. Chem.* **2008**, *47*, 4319–4328. (c) Zi, G.; Xiang, L.; Song, H. *Organometallics* **2008**, *27*, 1242–1246.
- (11) Manna, K.; Kruse, M. L.; Sadow, A. D. *ACS Catal.* **2011**, *1*, 1637–1642.
- (12) (a) Martinez, P. H.; Hultsch, K. C.; Hampel, F. *Chem. Commun.* **2006**, 2221–2223. (b) Ogata, T.; Ujihara, A.; Tsuchida, S.; Shimizu, T.; Kaneshige, A.; Tomioka, K. *Tetrahedron Lett.* **2007**, *48*, 6648–6650. (c) Deschamp, J.; Collin, J.; Hannedouche, J.; Schulz, E. *Eur. J. Org. Chem.* **2011**, 3329–3338.
- (13) (a) Buch, F.; Harder, S. Z. *Naturforsch.* **2008**, *63b*, 169–177. (b) Horrillo-Martínez, P.; Hultsch, K. C. *Tetrahedron Lett.* **2009**, *50*, 2054–2056. (c) Neal, S. R.; Ellern, A.; Sadow, A. D. *J. Organomet. Chem.* **2011**, *696*, 228–234. (d) Wixey, J. S.; Ward, B. D. *Chem. Commun.* **2011**, 47, 5449–5451. (e) Wixey, J. S.; Ward, B. D. *Dalton Trans.* **2011**, 40, 7693–7696. (f) Zhang, X.; Emge, T. J.; Hultsch, K. C. *Angew. Chem., Int. Ed.* **2012**, *51*, 394–398.
- (14) Knight, P. D.; Munslow, I.; O'Shaughnessy, P. N.; Scott, P. *Chem. Commun.* **2004**, 894–895.
- (15) Watson, D. A.; Chiu, M.; Bergman, R. G. *Organometallics* **2006**, *25*, 4731–4733.
- (16) (a) Wood, M. C.; Leitch, D. C.; Yeung, C. S.; Kozak, J. A.; Schafer, L. L. *Angew. Chem., Int. Ed.* **2007**, *46*, 354–358. (b) Ayinla, R. O.; Gibson, T.; Schafer, L. L. *J. Organomet. Chem.* **2011**, *696*, 50–60.
- (17) Gott, A. L.; Clarke, A. J.; Clarkson, G. J.; Scott, P. *Organometallics* **2007**, *26*, 1729–1737.
- (18) Zi, G.; Zhang, F.; Xiang, L.; Chen, Y.; Fang, W.; Song, H. *Dalton Trans.* **2010**, 39, 4048–4061.
- (19) Reznichenko, A. L.; Hultsch, K. C. *Organometallics* **2010**, *29*, 24–27.
- (20) (a) Reznichenko, A. L.; Emge, T. J.; Audörsch, S.; Klauber, E. G.; Hultsch, K. C.; Schmidt, B. *Organometallics* **2011**, *30*, 921–924. (b) Zhang, F.; Song, H.; Zi, G. *Dalton Trans.* **2011**, 40, 1547–1566.
- (21) (a) Gott, A. L.; Clarke, A. J.; Clarkson, G. J.; Scott, P. *Chem. Commun.* **2008**, 1422–1424. (b) Gott, A. L.; Clarkson, G. J.; Deeth, R. J.; Hammond, M. L.; Morton, C.; Scott, P. *Dalton Trans.* **2008**, 2983–2990.
- (22) (a) Shen, X.; Buchwald, S. L. *Angew. Chem., Int. Ed.* **2010**, *49*, 564–567. (b) Turnpenny, B. W.; Hyman, K. L.; Chemler, S. R. *Organometallics* **2012**, *31*, 7819–7822.
- (23) (a) Gagne, M. R.; Marks, T. J. *J. Am. Chem. Soc.* **1989**, *111*, 4108–4109. (b) Gagne, M. R.; Stern, C. L.; Marks, T. J. *J. Am. Chem. Soc.* **1992**, *114*, 275–294.
- (24) Hangaly, N. K.; Petrov, A. R.; Rufanov, K. A.; Harms, K.; Elfferding, M.; Sundermeyer, J. *Organometallics* **2011**, *30*, 4544–4554.
- (25) Stubbert, B. D.; Marks, T. J. *J. Am. Chem. Soc.* **2007**, *129*, 6149–6167.
- (26) Dunne, J. F.; Fulton, D. B.; Ellern, A.; Sadow, A. D. *J. Am. Chem. Soc.* **2010**, *132*, 17680–17683.
- (27) (a) Crimmin, M. R.; Arrowsmith, M.; Barrett, A. G. M.; Casely, I. J.; Hill, M. S.; Procopiou, P. A. *J. Am. Chem. Soc.* **2009**, *131*, 9670–9685. (b) Arrowsmith, M.; Crimmin, M. R.; Barrett, A. G. M.; Hill, M. S.; Kociok-Köhn, G.; Procopiou, P. A. *Organometallics* **2011**, *30*, 1493–1506. (c) Brinkmann, C.; Barrett, A. G. M.; Hill, M. S.; Procopiou, P. A. *J. Am. Chem. Soc.* **2011**, *134*, 2193–2207.
- (28) Liu, B.; Roisnel, T.; Carpentier, J.-F.; Sarazin, Y. *Angew. Chem., Int. Ed.* **2012**, *51*, 4943–4946.
- (29) (a) Pohlki, F.; Doye, S. *Angew. Chem., Int. Ed.* **2001**, *40*, 2305–2308. (b) Müller, C.; Saak, W.; Doye, S. *Eur. J. Org. Chem.* **2008**, 2731–2739. (c) Janssen, T.; Severin, R.; Diekmann, M.; Friedemann, M.; Haase, D.; Saak, W.; Doye, S.; Beckhaus, R. *Organometallics* **2010**, *29*, 1806–1817.

(30) Allan, L. E. N.; Clarkson, G. J.; Fox, D. J.; Gott, A. L.; Scott, P. J. *Am. Chem. Soc.* **2010**, *132*, 15308–15320.

(31) (a) Leitch, D. C.; Platel, R. H.; Schafer, L. L. *J. Am. Chem. Soc.* **2011**, *133*, 15453–15463. (b) Leitch, D. C.; Payne, P. R.; Dunbar, C. R.; Schafer, L. L. *J. Am. Chem. Soc.* **2009**, *131*, 18246–18247.

(32) Manna, K.; Ellern, A.; Sadow, A. D. *Chem. Commun.* **2010**, *46*, 339–341.

(33) Tobisch, S. *Chem.—Eur. J.* **2011**, *17*, 14974–14986.

(34) Gribkov, D. V.; Hultsch, K. C. *Angew. Chem., Int. Ed.* **2004**, *43*, 5542–5546.

(35) (a) Walsh, P. J.; Hollander, F. J.; Bergman, R. G. *J. Am. Chem. Soc.* **1988**, *110*, 8729–8731. (b) Baranger, A. M.; Walsh, P. J.; Bergman, R. G. *J. Am. Chem. Soc.* **1993**, *115*, 2753–2763. (c) Straub, B. F.; Bergman, R. G. *Angew. Chem., Int. Ed.* **2001**, *40*, 4632–4635.

(36) (a) Kissounko, D. A.; Epshteyn, A.; Fettinger, J. C.; Sita, L. R. *Organometallics* **2006**, *25*, 1076–1078. (b) Leitch, D. C.; Schafer, L. L. *Organometallics* **2010**, *29*, 5162–5172.

(37) Majumder, S.; Odom, A. L. *Organometallics* **2008**, *27*, 1174–1177.

(38) Leitch, D. C.; Turner, C. S.; Schafer, L. L. *Angew. Chem., Int. Ed.* **2010**, *49*, 6382–6386.

(39) Katayev, E.; Li, Y.; Odom, A. L. *Chem. Commun.* **2002**, 838–839.

(40) (a) Neukom, J. D.; Perch, N. S.; Wolfe, J. P. *J. Am. Chem. Soc.* **2010**, *132*, 6276–6277. (b) Neukom, J. D.; Perch, N. S.; Wolfe, J. P. *Organometallics* **2011**, *30*, 1269–1277.

(41) (a) Tye, J. W.; Hartwig, J. F. *J. Am. Chem. Soc.* **2009**, *131*, 14703–14712. (b) Hanley, P. S.; Markovic, D.; Hartwig, J. F. *J. Am. Chem. Soc.* **2010**, *132*, 6302–6303.

(42) Casalnuovo, A. L.; Calabrese, J. C.; Milstein, D. *J. Am. Chem. Soc.* **1988**, *110*, 6738–6744.

(43) Manna, K.; Xu, S.; Sadow, A. D. *Angew. Chem., Int. Ed.* **2011**, *50*, 1865–1868.

(44) Dunne, J. F.; Manna, K.; Wiench, J. W.; Ellern, A.; Pruski, M.; Sadow, A. D. *Dalton Trans.* **2010**, *39*, 641–653.

(45) Kidd, R. G. *Boron-11*; Academic Press: New York, 1983; Vol. 2.

(46) (a) Herberich, G. E.; Fischer, A. *Organometallics* **1996**, *15*, 58–67. (b) Roitershtein, D.; Domingos, Å.; Marques, N. *Organometallics* **2004**, *23*, 3483–3487.

(47) Dunne, J. F.; Su, J.; Ellern, A.; Sadow, A. D. *Organometallics* **2008**, *27*, 2399–2401.

(48) (a) Ralevic, V. *Eur. J. Pharmacol.* **2003**, *472*, 1–21. (b) Nicolaou, K. C.; Roecker, A. J.; Pfefferkorn, J. A.; Cao, G.-Q. *J. Am. Chem. Soc.* **2000**, *122*, 2966–2967. (c) Sun, H.; Moore, C.; Dansette, P. M.; Kumar, S.; Halpert, J. R.; Yost, G. S. *Drug Metab. Dispos.* **2009**, *37*, 672–684. (d) Gueritte, F.; Fahy, J. In *Anticancer Agents from Natural Products*; Cragg, G. M., Kingston, D. G. I., Newman, D. J., Eds.; CRC Press: Boca Raton, FL, 2005; pp 123–135.

(49) (a) Kuwano, R.; Kashiwabara, M. *Org. Lett.* **2006**, *8*, 2653–2655. (b) Kuwano, R.; Kashiwabara, M.; Sato, K.; Ito, T.; Kaneda, K.; Ito, Y. *Tetrahedron: Asymmetry* **2006**, *17*, 521–535.

(50) Arp, F. O.; Fu, G. C. *J. Am. Chem. Soc.* **2006**, *128*, 14264–14265.

(51) Jung, M. E.; Piizzi, G. *Chem. Rev.* **2005**, *105*, 1735–1766.

(52) The k' value is calculated from a linear least-squares regression analysis of k_{obs} vs $[\{S-2\}Zr(NMe_2)_2]$.

(53) For group 4 catalysts that show product inhibitions and/or nonlinear kinetics, see refs 25 and 31.

(54) For rare earth catalysts that show product inhibition and nonlinear kinetics, see refs 3b, 6d, and (a) Li, Y.; Marks, T. J. *J. Am. Chem. Soc.* **1996**, *118*, 9295. (b) Hong, S.; Kawaoka, A. M.; Marks, T. J. *J. Am. Chem. Soc.* **2003**, *125*, 15878. (c) Ryu, J. S.; Li, G. Y.; Marks, T. J. *J. Am. Chem. Soc.* **2003**, *125*, 12584.

(55) Cornish-Bowden, A. *Fundamentals of Enzyme Kinetics*, 3rd ed.; Portland Press: London, 2004.

(56) (a) Tobisch, S. *Dalton Trans.* **2012**, *41*, 9182–9191. (b) Tobisch, S. *Inorg. Chem.* **2012**, *51*, 3786–3795.